VAPOR-PHASE DETECTION OF EXPLOSIVES

BY SURFACE-ENHANCED RAMAN SCATTERING

By

SUMEDHA TAMANE

Bachelor of Technology in Mechanical Engineering

Jawaharlal Nehru Technological University

Hyderabad, Andhra Pradesh, India

2008

Submitted to the Faculty of the
Graduate College of the
Oklahoma State University
in partial fulfillment of
the requirements for
the Degree of
MASTER OF SCIENCE
December, 2011

VAPOR-PHASE DETECTION OF EXPLOSIVES

BY SURFACE-ENHANCED RAMAN SCATTERING

Thesis Approved:

Dr. A. Kaan Kalkan

Thesis Adviser

Dr. David A. Rubenstein

Committee Member

Dr. Kevin Ausman

Committee Member

Dr. Sheryl. A. Tucker

Dean of the Graduate College

TABLE OF CONTENTS

Table of Contents iii

List of Tables v

List of Figures vi

1. Introduction 1

2. Literature Review 5
2.1 Overview 5
2.2 Trinitrotoluene 5
2.3 Current Explosives Detection Techniques 9
2.3.1 X-ray Systems 10
2.3.2 Millimeter wave technology 10
2.3.3 Gas Chromatography (GC) 12
2.3.4 Ion-Mobility Spectroscopy (IMS) 12
2.4 Raman Spectroscopy 14
2.5 Surface Enhanced Raman Scattering (SERS) 16
2.6 Enhancement mechanisms in SERS 17
2.7 SERS substrates 19
2.8 Advantages of SERS over other techniques 20
2.9 Previous work on explosives detection using SERS 21

3. Methodology 23
3.1 Overview 23
3.2 Silicon thin film deposition 23
3.3 Analyte 24
3.4 Nanoparticle synthesis 24
3.5 Exposing the nanoparticles to TNT vapor 26
3.6 SERS Acquisitions 28
3.7 Nanoparticle temperature measurement using Raman Spectroscopy 29

4. Results and Discussion 31
4.1 Overview 31
4.2 Physical characterization of SERS substrate 32
4.2.1 Atomic Force Microscopy 32

4.2.2 UV-Visible spectroscopy 33
4.3 SERS of TNT vapor and Raman of TNT simulant 35
4.4 Different adsorption configurations of TNT 36
4.5 Temperature of silver nanoparticles 43
4.6 SERS of TNT in ambient air 44
4.7 SERS of TNT in pure oxygen environment 46
4.8 Effect of water vapor on SERS of TNT 47
4.9 SERS of TNT in the presence of 20% RH argon 49
4.10 SERS of TNT in dry air 50
4.11 Vapor phase detection of RDX and PETN 51

5. Conclusions 52

Bibliography 55

LIST OF TABLES

Table 4.1. Raman peaks for TNT and their designation.....36

LIST OF FIGURES

Figure 2.1. Production of TNT using three step nitration process.....7

Figure 2.2. Skeletal structure of TNT molecule 8

Figure 2.3. Holographic image of subject in millimeter wave portal 11

Figure 2.4. Commercially available Ion Mobility Spectrometer 13

Figure 2.5. Energy level diagram illustrating Rayleigh and Raman scattering. Thickness of lines indicate the signal strength of different mechanisms of scattering.....15

Figure 3.1. Synthesis of silver nanoparticles on silicon film.....25

Figure 3.2. Schematic representation of the SERS substrate inside the optical cell....26

Figure 3.3. Experimental set up for purging of the optical cell 27

Figure 3.4. Graphical illustration of SERS acquisitions 28

Figure 4.1. Representative AFM image of the Ag nanoparticles on the SERS substrate 32

Figure 4.2. Extinction spectrum of Ag nanoparticles on Si film synthesized by immersion in 2 mM $AgNO_3$ + 0.1 % HF for 30 s.....34

Figure 4.3. SERS of TNT vapor and Raman scattering of TNT simulant.....35

Figure 4.4. SERS spectra of all possible fragments of TNT.....38

Figure 4.5. Time series spectra of TNT captured for the first 50 s in 11 s intervals ...39

Figure 4.6. TNT molecules adsorbed to Ag in “standing up” and “lying down” configurations 40

Figure 4.7. Time series SERS spectra of TNT captured at intervals of 11 s 41

Figure 4.8. Normalized intensity increase of the SERS baseline (adopted as 1360 cm^{-1}) and normalized intensity reduction of the 825 cm^{-1} peak as a function of time. Series correspond to 11 s intervals 42

Figure 4.9. (a) Anti-Stokes and (b) Stokes Raman scattering spectra of FBT.....43

Figure 4.10. SERS spectra of TNT vapor in argon and ambient air.....44

Figure 4.11. SERS of TNT in ambient air followed by argon.....45

Figure 4.12. SERS spectrum of TNT in O_2 environment 46

Figure 4.13. SERS spectra of TNT in O_2 and 1,3,5 TNB in argon.....47

Figure 4.14. SERS of TNT in argon and 100% RH.....48

Figure 4.15. SERS of TNT in the presence of 20% RH argon 49

Figure 4.16. SERS of TNT in dry air ambient.....50

Figure 4.17. SERS and Raman spectra of RDX and PETN.....51

CHAPTER 1

INTRODUCTION

Global terrorism has become a major issue of concern due to the increasing use of Improvised Explosive Devices (IEDs) in suicide bombing. IEDs are becoming popular as they are easy to hide and transport. Some of the most significant acts of terrorism in the past are; the attack on Jerusalem in August 2001, involving an IED concealed in a guitar carried by a suicide bomber, the suicide attack on Baghdad in June 2006, involving a shoe-bomber carrying explosives and ball-bearings inside his shoes, and the terrorist attack on a flight from Amsterdam to Detroit in December 2009, involving an explosive device containing PETN hidden in the underpants of the terrorist. These threats have compelled researchers to modify and update the explosive detection methods. There is an urgent need to detect explosives at trace level and at standoff distance in order to minimize such activities. Various explosives like TNT, PETN, RDX, and TNB are used in terrorism. TNT is considered as a standard explosive because of its high explosive power, convenient handling properties, and less sensitivity to shock and friction. TNT is listed as a Class C potential human carcinogen and is also known to cause anemia, jaundice, gastritis, cyanosis, enlarged spleen, cataracts, and hepatitis [1, 2].

Detection of explosives at airports and other public places is a challenging task because of interference caused by the dynamic background and the risk of false alarms. Currently deployed X-ray machines provide only imagery of the scanned items rather than a detailed chemical analysis of the contents. Techniques based on density images provide insufficient data making it difficult to differentiate between non-hazardous items having density similar to that of explosives. Therefore, for successful detection of explosives spectroscopic techniques which distinguish them on the basis of their detailed fingerprint signals are needed. At present, Ion-mobility Spectroscopy (IMS) is extensively used for trace detection of explosives [3, 4]. It can be used in either particulate or vapor detection modes. The sampling is achieved by either swiping over a surface to collect particles of explosives or drawing air from the surroundings of the object. Subsequently, the sample is delivered into the ionization region of the detector where electrons interact with incoming explosive molecules and produce negative ions. An electric field swipes these ions into a drift region of the IMS. The time required by the ions to move through the drift region is known as ‘drift-time’. Drift-time is generally in the order of milliseconds and is a complex function of mass, charge and size of the ion [4]. The disadvantage of IMS is that if two different materials form ions of similar size, the spectrum appears as a single broad peak rather than two distinct peaks. Therefore, it is important that a trace detection system produces information based on the structure of the molecule. Conventional spectroscopic techniques like Raman spectroscopy and infrared spectroscopy produce a definite “finger-print” for a molecule. These techniques are limited to bulk detection only. On the other hand, the vapor pressure of most of the explosives is in the range of 1-10 ppb. Therefore, detection technologies of interest based

upon vapor of explosives are required to have trace level sensitivities. Surface-enhanced Raman Scattering (SERS) has emerged as an ultrasensitive analytical technique with the potential to detect traces of explosives. The spectrum obtained is the molecule's vibrational signature and offers the highest capability to distinguish between different molecules ruling out the interferents. Previous investigations on SERS of explosives involved either solution or powder samples, while reports on detection in vapor phase are limited and not conclusive [5-8].

In the present work, we demonstrate vapor phase detection of Trinitrotoluene (TNT) at concentrations on the order of few ppb for the first time using a SERS substrate approach. Indigenously prepared "nanometal-on-semiconductor" SERS substrates developed by Kalkan and co-workers [9, 10] are employed in this work. The substrates were prepared by chemical reduction of 2 mM Ag^{+} on plasma-deposited Si thin films, resulting in monolayers of surfactant-free Ag nanoparticles. Nanoparticle charging is a useful attribute of this approach which is responsible for self-inhibition of the chemical reduction [9]. Coalescence can be avoided despite few nm of interparticle spacing resulting in pronounced plasmon hybridization. Hence, high enhancement factor SERS substrates can be realized.

We have identified that vapor phase detection of explosives was limited in the past because of three major challenges: 1) low vapor pressures of explosives at room temperature; 2) weak adsorption of the explosives on silver nanostructures that accounts for easy desorption even under low laser excitation; and 3) chemical decomposition of the explosives under laser exposure. Explosives detection by SERS is also complicated by different adsorption configurations of the explosive molecule. In particular, the

present research has revealed the different adsorption configurations of TNT on Ag nanoparticles using SERS selection rules. The different adsorption configurations are associated with different desorption rates or decomposition rates during the SERS acquisition. We understand that desorption and decomposition of the explosives are the major reasons, which have hindered SERS of explosives in vapor phase; previously.

The organization of the present thesis is as follows: Chapter 2 reviews the structure of TNT, currently used explosive detection systems, phenomena of Raman scattering and SERS. In Chapter 3, procedures for substrate preparation, nanoparticle synthesis and characterization methods are described. Chapter 4 presents the results obtained in the present work. Particularly, the SERS spectrum of TNT shows different adsorption configurations of TNT. SERS spectrum of TNT is compared with its Raman spectrum and kinetics of major SERS peaks is studied. The SERS spectra of various fragments that could possibly be formed during decomposition of TNT are also provided. Also, the temperature of the nanoparticles under the conditions of SERS acquisition was measured using the Raman spectroscopy. Finally, Chapter 5 concludes the present study.

CHAPTER 2

LITERATURE REVIEW

2.1 Overview

This Chapter provides a review on the structure of Trinitrotoluene (TNT) molecule and currently used explosive detection techniques. It also presents the background on fundamentals of Raman scattering and Surface-enhanced Raman Scattering (SERS). Advantages of SERS over other techniques and an account of previous works on SERS of TNT are also reviewed.

2.2 Trinitrotoluene

Explosives are chemically unstable compounds that contain large amount of stored energy and do not require external oxygen for decomposition. When exposed to external heat or mechanical shock, explosives rearrange their molecular structure and expand spontaneously. This spontaneous detonation propagates in the form of high speed shock waves and release high energy. Special explosives called permissible explosives

may also be used in peaceful applications like mining, quarrying, rocket launching, and avalanche control. Explosives are classified based on their chemical structure, and the most threatening explosives are organic compounds containing the nitro group. Based on the nitro group, explosives are classified as aliphatic nitrate esters (R-O-NO_2), cycloaliphatic nitramines (>N-NO_2), and nitro aromatics (Ar-NO_2) [11]. By identifying the symmetric and asymmetric NO_2 bands in their vibrational spectra, nitro-containing explosives and non-nitro containing compounds can be clearly distinguished.

TNT belongs to nitro-aromatic group of explosives [11]. It is a secondary explosive and can be used by itself or mixed with other explosives. TNT is a yellow crystalline solid that does not occur naturally in the environment. It was first synthesized in 1863 by a German Chemist, Joseph Wilbrand using toluene, sulphuric acid, and nitric acid as raw materials. TNT is prepared by three-step nitration of toluene using batch process or continuous process as shown in Fig. 2.1 [12-14]. In the first stage, the mixed acid stream counterflows to the toluene stream. 2-Nitrotoluene (2-NT) and 4-Nitrotoluene (4-NT) formed after the first step is subjected to further nitration. In the second stage of nitration, 2, 4 Dinitrotoluene (2, 4 DNT) and 2, 6 Dinitrotoluene (2, 6 DNT) are produced. DNTs are treated with HNO_3 and oleum (sulfur trioxide in anhydrous sulfuric acid) to produce 2, 4, 6 TNT and other isomers of TNT. Crude TNT produced from nitration is washed with water to remove traces of acid, and is neutralized with soda ash. Aqueous sodium sulfite solution (Stellite) is used to remove the contaminating isomers [12-14].

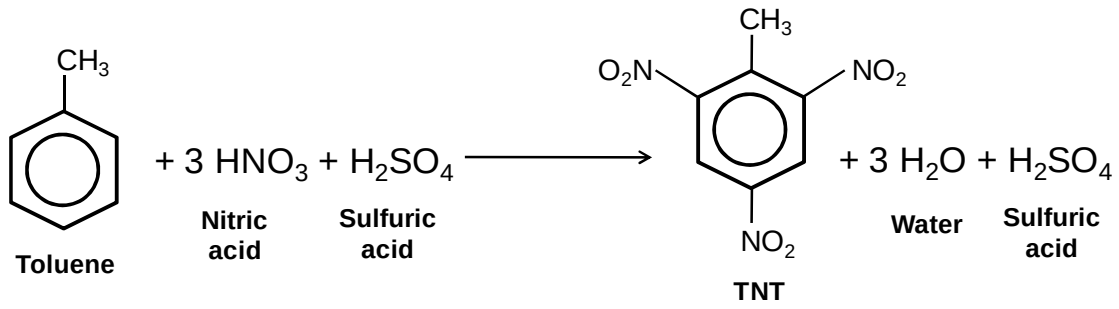

Figure 2.1. Production of TNT using three step nitration process [12].

TNT was initially used as a dye until its explosive potential was realized thirty years later. It has low solubility in water but dissolves in most organic solvents. The solubility of TNT in water varies from 100-200 mg/L at room temperature [15-17]. TNT has a melting point of 80.4 °C, a density of 1.58 g /cm^3, and a detonation velocity of 6700 ms^{-1}, [18]. The vapor pressure of TNT, at room temperature is ~ 3 ppb [19]. TNT is superior to other explosives because of its high explosive power, convenient handling properties due to high stability, and less sensitivity to shock and friction which reduces the risk of accidental detonation.

X-ray studies on the structure of TNT have revealed the existence of two crystallographic forms; monoclinic and orthorhombic [20-23]. Theoretical calculations of the TNT structure performed using B3LYP/6-31G* and B3LYP/6-311+G** density functional methods resulted in two minimum energy structures [23]. The geometry of the low energy structure closest to the crystal structure of TNT shows that one of the methyl hydrogen atoms is perpendicular to the phenyl ring.

Also, the 4-nitro group is planar with the phenyl ring and the 2, 6-nitro groups are non-planar with the phenyl ring due to the steric hindrance between the methyl and nitro groups [23, 24]. Figure 2.2 shows the ball and stick model of TNT molecule.

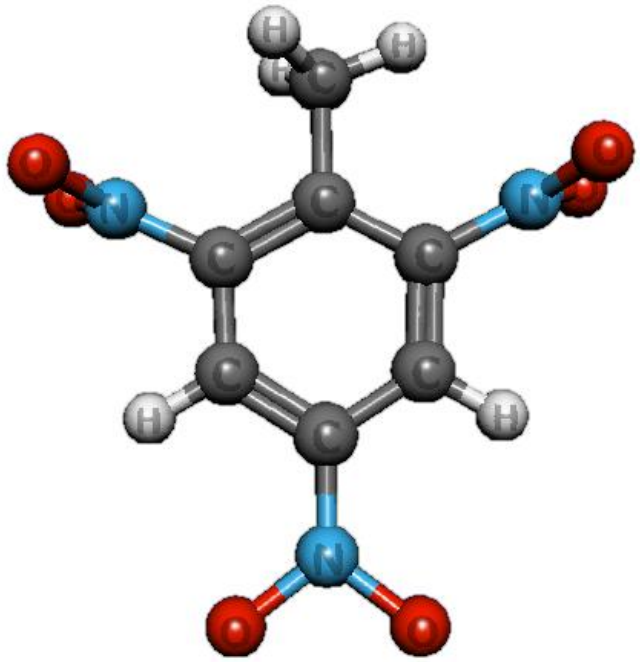

Figure 2.2. Skeletal structure of TNT molecule.

Incomplete burning of TNT and improper disposal of large concentrations of waste has led to significant contamination of soil and water throughout the world during World-War II. TNT is introduced into the environment due to several reasons such as manufacturing of the compound, transport and detonation of bombs, and storage of TNT explosives. TNT is listed as a Class C potential human carcinogen and is also known to cause anemia, jaundice, gastritis, cyanosis, enlarged spleen, cataracts, and hepatitis [1, 2]. Effective detection techniques have to be established bearing in mind the environmental risks and particularly the increasing terrorist attacks caused by explosives.

Explosives detection in vapor phase is difficult because of its low vapor pressure. Therefore, detection methods that rely on air samples need either large volume of the samples or exceedingly high detection sensitivity. Also, explosives are usually packed using materials that further block the escape of explosive vapors. Even if techniques are established to increase the vapor pressure of explosives by increasing the temperature, thermal degradation of the material occurs which complicates the detection process [3]. Currently used commercial sensors are based on different techniques, such as Ion-mobility Spectroscopy, Gas Chromatography, Raman scattering, UV/Visible method, and electronic nose devices.

2.3 Current Explosive Detection Techniques

Currently used explosive detection techniques can be broadly categorized into two; image detection and trace detection. In imaging techniques, images of personnel and hand carried or checked luggage in aviation are produced by irradiating the body with X-rays or millimeter waves, and analyzing the radiation back-scattered from the body. Hidden objects on the human body reflect different radiations thus producing distinct images for metallic and non-metallic objects on the body [4]. In trace-level detection, chemical analysis is performed on the sampled air or residues obtained from clothes or bodies of individuals. Trace-level detection technique is capable of detecting even low amounts of explosives and avoids the risk of false alarms. Some of the imaging and trace level detection techniques have been reviewed in the following sections.

2.3.1 X- ray systems

X-ray based systems are commonly used in airports to scan the luggages. The object is placed before the scanner for several seconds and the front and rear sides of the object are scanned. The intensity of the X-rays back scattered from each location on the body are used to produce an electronic image. The X-ray scatter intensity is a function of atomic number and density of the material [4]. In systems using high energy X-rays, the adsorbed energy primarily depends on the material density. Metals having high density absorb more X-rays and appear as dark areas while clothing and hair on the human body appear transparent on the image. Objects concealed behind the metal accessories present on the body are difficult to be traced because of the dark areas on the images [4]. As a solution to this problem, a dual-energy X-ray system was developed wherein, an additional low energy X-ray was employed [25]. At lower energies the absorption mainly depends upon the atomic number and thickness of the material. Low atomic number materials like drugs and explosives are good scatterers of X-ray and appear as bright areas on the image. By comparing the high and low energy views, explosives and other harmful objects can be traced. The disadvantage of this technique is that the real density of the luggage is unknown and the system generates an approximate atomic number for the material, which may result in lethal item to be mistaken for a non-hazardous one.

2.3.2 Millimeter wave technology

Millimeter waves are high-frequency electromagnetic waves within the frequency band of 30-300 GHz. Millimeter wave systems are non-ionizing and do not cause any health hazards at low power levels. These systems have high resolution and allow

discrimination between objects because of a short wavelength range (1-10 mm) [26, 27]. Concealed items are detected by illuminating a person by millimeter-wave transceiver at low power. These waves easily penetrate into clothing material whereas reflect from the human body and other hidden weapons. In this technique, a holographic system is used along with a millimeter-wave transmitter receiver, a high-speed digital signal processor, a cylindrical scanner and a holographic image algorithm. This is a coherent system and operates at a single frequency. The phase and the amplitude of the returned signal are recorded and reconstructed into an image using a computer [27]. Figure 2.3 shows a sample holographic image in millimeter wave portal. The advantages of this system include high resolution, near real-time operation, and a full body field view [26, 27]. However, along with the detection of concealed items, the human physical features are also displayed and due to privacy concerns this technique is not implemented at airport checkpoints.

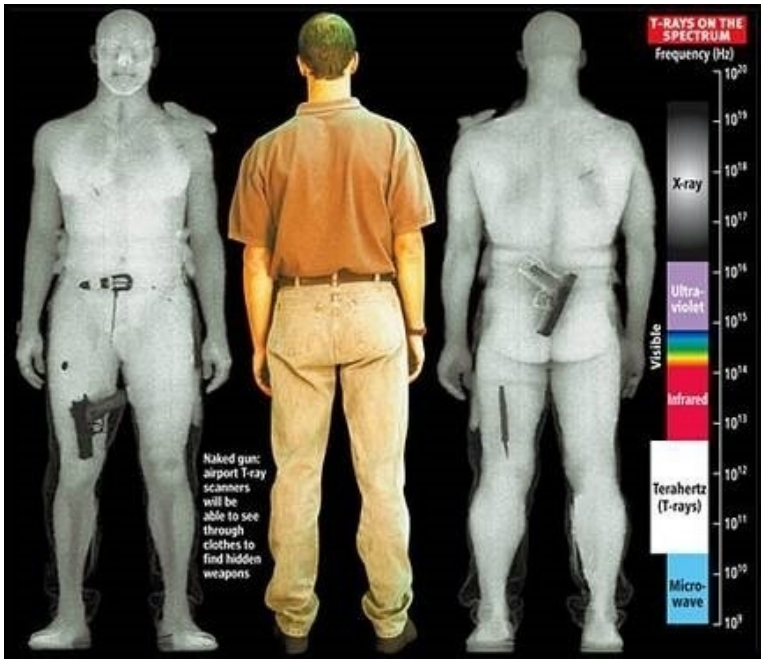

Figure 2.3. Holographic image of subject in millimeter wave portal.

2.3.3 Gas chromatography (GC)

Chromatographic methods are used for separating the components of a gaseous sample between two phases. The first phase is a stationary bed with large surface area and the second phase is a mobile phase that percolates through the stationary bed. The sample is pushed through the column using a carrier gas usually helium or argon. Various components of the sample interact differently with the stationary phase in the column and emerge out at different 'retention times' and the sample gas are thus separated [28]. Subsequently, the separated components are detected using a device whose intensity is proportional to concentration of the component in the mixture. The commonly used detection systems are Electron-Capture Detector (ECD), Thermal Energy Analyzer (TEA), mass spectroscopy, and Surface Acoustic Wave (SAW). For direct separation of liquid samples, High Performance Liquid Chromatography (HPLC) is used [3]. Environmental Protection Agency (EPA) Method 8330 is the standard method for trace explosive residue detection of Nitroaromatics and Nitramines that uses HPLC separation and UV detection [29]. The advantages of gas chromatography are that it is an inexpensive, reliable and relatively simple technique with fast and non-destructive analysis, and high resolution. However, this technique is limited to volatile samples and is not suitable for thermally liable samples. Also, the sensitivity of GC is limited to low ppm levels.

2.3.4 Ion Mobility Spectroscopy (IMS)

IMS is the most successful technique used for trace detection of explosives. In this technique, two independent principles are combined to produce a speed response toward gas or vapor species present on hand bags and carry-on luggages. This system

consists of a sample inlet, an atmospheric pressure ion source, an ion gate, a drift region, and a detector. The ion gate electronically injects ions from the source into the drift region in the form of discrete packets [30]. The drift tube is isolated from atmospheric air and the ions are accelerated along the tube by a uniform weak electric field present inside the tube. As the ions travel through the drift region, they are separated according to their mobility which is dependent on the mass/charge ratio. The movement of these ions toward the detector is hindered because of their collisions, and depending on the ion impact a current is generated, which is measured over the time of flight. The output produces a spectrum of ion current versus time of ion drift [3, 30, 31]. Figure 2.4 shows IONSCAN 400B, a commercially available desktop narcotic and explosive detector based on the IMS technology manufactured by Smiths Detection Inc. [32].

Figure 2.4. Commercially available Ion Mobility Spectrometer [32].

The major problem with IMS system is that it does not allow quantification. Also, these systems suffer from production of false alarms due to non-explosive materials and masking in the presence of other species in the environment. IMS works best when combined with additional analytical methods. Another problem with explosives detection using IMS is the production of fragment ions which compromises with the specificity of this method [3, 30]. For example, if two components form ions of similar size and mass, then instead of two peaks one single broad peak appears in the IMS spectrum. To avoid this problem, spectrometric techniques that produce a spectrum unique to every molecule are required.

2.4 Raman Spectroscopy

Raman Spectroscopy is a light scattering technique based on the phenomenon of change in frequency of light when scattered by molecules. This phenomenon was first predicted theoretically by Smekal [33] in 1923 and was experimentally demonstrated by C.V Raman and K.S Krishnan [34] in 1928. The same effect was observed on quartz by Landsberg and Mandelstam [35].

When a monochromatic light irradiates a substance, most of the photons are scattered from the surface elastically (without energy change) giving rise to Rayleigh scattering [36]. In addition to Rayleigh scattering, inelastic scattering of the light occurs known as Raman scattering. The amount of energy change involved in the transition of scattering species corresponds to the Raman shift equals the energy of a vibrational mode unique to the molecule and therefore, every molecule has a unique Raman spectrum [36]. During light scattering, an electron is excited from the ground state to a virtual state by the incident light as shown in Fig. 2.5. Subsequently, if this electron returns to the same

ground state, a photon is emitted having energy same as that of incident photon. This phenomenon is called Rayleigh scattering. On the other hand, the excited electron may return to a vibronic state (which represents the coupling of electronic state with a vibrational state) instead of the ground state as shown in Fig. 2.5. The emitted photon in this case has energy less than that of incident photon which results in creation of a phonon. This type of scattering is known as Stokes Raman scattering [36, 37]. Also, the electron may get excited from the vibronic state and return to the ground state as shown in Fig. 2.5. In this case, the emitted photon has energy greater than the incident photon resulting in annihilation of a phonon. This event gives rise to anti-Stokes Raman scattering [36, 37].

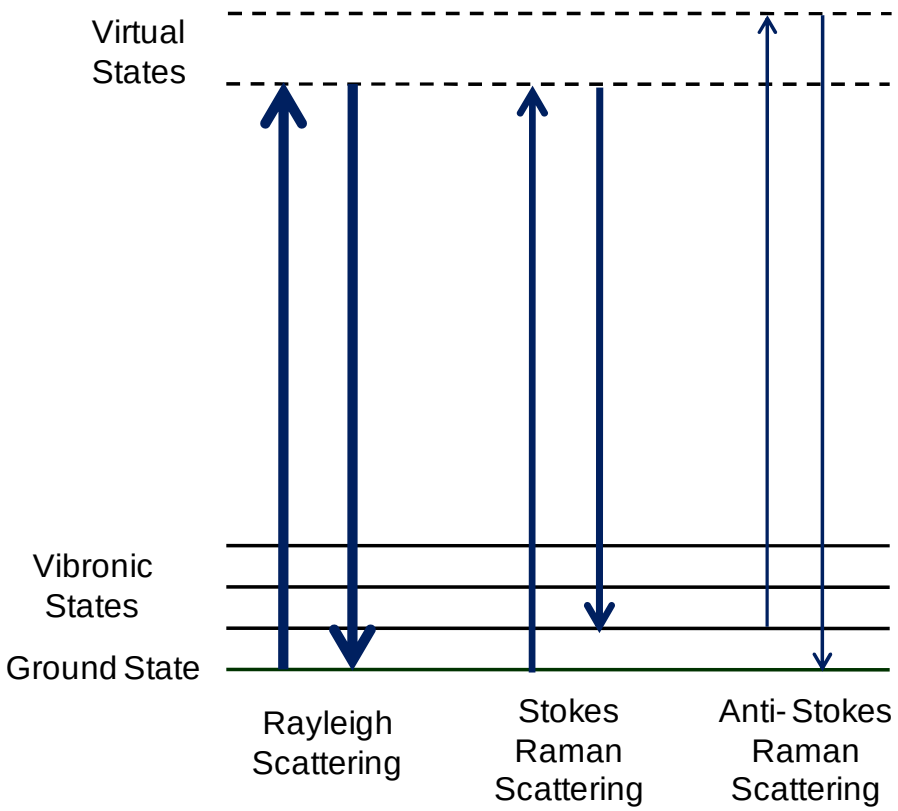

Figure 2.5. Energy level diagram illustrating Rayleigh and Raman scattering. Thickness of lines indicates the signal strength of different mechanisms of scattering.

Raman spectroscopy is being applied in various fields for analysis of materials and systems. Some of the areas of application are pharmaceutical industry [38], gemology [39], quality control of thin films and polymers, and petroleum analysis. In the field of Bioscience, Raman spectroscopy is used to distinguish between harmful and normal tissues. Although Raman spectroscopy has several applications, it is limited to bulk materials and cannot be effectively used at the trace level because of small Raman cross-sections (10^{-30} to 10^{-25} cm^2 per molecule) [40] which require large number of analyte molecules. Another limitation is the interference from fluorescence background which reduces the intensity of the Raman signal. Also, because of its low sensitivity, this technique demands the use of powerful and expensive lasers.

2.5 Surface Enhanced Raman Scattering

SERS effect amplifies the Raman signal by several orders of magnitude (~10^{15}). It is a surface technique wherein the molecules are either adsorbed on or in close proximity of the metal surface. SERS phenomenon was first observed by M. Fleischmann *et al*. [41] in 1974. They observed an anomalous increase in the Raman signal from pyridine adsorbed on roughened silver electrode surface, and attributed it to the increased surface area of the rough substrate. Later, two independent groups Jeanmarie and Van Duyne [42] and Albrecht and Creighton [43] demonstrated the result of Fleishmann. However, these groups suggested that the enhancements could not occur by simple increase in the number of scatterers present, but the phenomenon occurred in the adsorbed state. Jeanmarie and Van Duyne proposed that the increase in the Raman intensity is an electromagnetic effect, while Albrecht and Creighton attributed it to electronic effect. Creighton and co-workers [43] also demonstrated that metal salt solutions of Ag, Au and

Cu exhibit surface plasmon bands in the visible region and are excellent choices for SERS studies. The emphasis of SERS technique lies in the key role played by these noble metal particles present on the substrate. This technique has been successfully applied for trace-level detection [44-46] and single molecule detection which produces enhancements in the order of 10^{13}-10^{15} [47-51]. The signal obtained from SERS is proportional to the Raman cross-section of the adsorbed molecule, the excitation laser intensity, the number of molecules involved in the SERS process, and effective enhancement factor [40]. The fundamental theory of enhancement in SERS is still a topic of debate. However, two major enhancement factors have been proposed in the literature; i.e., chemical enhancement and electromagnetic enhancement [52-54]. Generally, both these mechanisms act simultaneously and produce multiplicative effects.

2.6 Enhancement mechanisms in SERS

SERS signals can be enhanced by two mechanisms: electronic (also referred to as chemical enhancement) and optical (also referred to as electromagnetic enhancement). Electromagnetic enhancement occurs in the vicinity of nanoparticles because of localized optical fields, produced as a result of electromagnetic resonances caused by coupling of surface plasmons with the incident photons [40, 53-55]. Plasmons are collective excitations that arise when light interacts with free electrons in a metal nanostructure whose size is significantly smaller than the wavelength of light. These plasmons, when confined to near-surface region, are called surface plasmons [55]. On surfaces of metal nanoparticles, the surface plasmon excitations cannot propagate, and they are called localized surface plasmons. The electromagnetic enhancement is generally of the order of 10^{4}-10^{7} [40, 56].

A simple electrostatic model can be considered to explain the localization of incident and scattered fields around a nanoparticle. When a localized surface plasmon is excited with a laser beam, the metal nanoparticle radiates a dipolar field. The induced dipole creates an electric field (E) along the dipole axis such that,

$$E \propto \frac{1}{d^3} \qquad 2.1$$

where, d is the distance from center of the dipole. A coherent interaction of the incoming electric field with the dipolar field of the plasmon redistributes the electric field intensity around the nanoparticles. The intensity of local radiation (I_{Local}) around the nanoparticle is directly proportional to the square of electric field.

$$I_{Local} \propto E^2 \propto \frac{1}{d^6} \qquad 2.2$$

This enhancement occurs for both incident and scattered radiation. The intensity of the scattered field, E_s is also proportional to the square of the incident light. The total intensity of the enhanced field, I_{SERS}, is the product of both incident and scattered fields [57]. Hence,

$$I_{SERS} \propto E_i^2 . E_s^2 \propto E^4 \propto \frac{1}{d^{12}} \qquad 2.3$$

where, E_i is the electric field of incident light and E_s is the electric field of scattered light. The enhancement is maximum for adsorbed molecules whose polarization axis is normal to the surface. No enhancement is observed in molecules whose axis is parallel to the surface.

Additionally, chemical effect also contributes to the SERS enhancement, though not as much as the electromagnetic enhancement. In the literature, two models have been proposed for the chemical enhancement mechanism. First, the presence of metal surface may increase the polarizability of the adsorbate which may in turn increase the Raman cross-section area [58]. Second, the electronic states of the adsorbate are broadened or shifted due to their interaction with the metal surface resulting in the resonant Raman effect [54].

2.7 SERS substrates

A metallic nanostructure that produces SERS enhancement is referred to as a SERS substrate. Apart from the optical system, the key to an enhanced SERS signal is production of an ideal metal surface. SERS enhancement critically depends on the nature of the metal and the surface roughness. SERS substrates are categorized into three classes: i) aggregated metal colloids generated by chemical methods; ii) metallic planar structures like arrays of metallic nanoparticles; iii) electrochemically roughened electrode surfaces [59]. A good SERS substrate typically exhibits enhancements only in a limited wavelength range, most often in the visible/near-infrared excitation range (400-1000 nm) [58]. Commonly used SERS substrates are metals such as silver, gold and copper as they fulfill the resonance condition in the visible/near-infrared region which is the frequency range of most lasers [60]. These metals at the nano scale (10-100 nm length scales) exhibit localized surface plasmons that can be excited with visible light [58]. In the past, several methods have been proposed for the preparation of metal nanostructured substrates for SERS using surfactant molecules. However, surfactants act as a barrier between the analyte and metal resulting in disappearance of surface-enhanced effects [9].

Chapter 3 describes the methodology used for preparation of surfactant-free SERS substrates employed in the present work.

2.8 Advantages of SERS over other techniques

SERS technology offers several advantages in terms of sensitivity and interferences over other competing technologies.

i. Most of the detection techniques used earlier provide only imagery of the screened items and no chemical analysis. SERS is a ‘fingerprint’ spectroscopic technique which discloses detailed information about the molecular structure of the analyte.

ii. In IMS, the drift-time measured by the system is not a direct property of the molecule but represents the interaction of the molecule with the measurement system. On the other hand, in SERS, the peaks directly correspond to the energies of the vibrational modes of a molecule, and even the smallest change in the structure, such as protonation or interaction with other molecules, causes a significant change in the spectrum. Also, SERS is useful not only to detect the explosives, but also to distinguish between the molecules, thus eliminating the possibility of interferents.

iii. The commercialization of SERS in general is challenged by issues like irreproducibility, low sensitivity, and high cost. But, the SERS substrates produced in this project are cost effective and less time consuming as the nanoparticles are synthesized by a single immersion step.

2.9 Previous work on explosive detection using SERS

K. Kneipp and coworkers [5] were the first to demonstrate SERS of TNT on colloidal silver and gold. The Raman measurements were performed using near-IR excitation. Solution of colloidal silver used in the experiment was prepared by standard citrate reduction procedure. To obtain maximum SERS signal, the colloidal gold solution was diluted in water. This work suggests two types of adsorption configurations of TNT on gold and silver. TNT molecules lay “flat” on the silver colloids due to selective chemical enhancement of the out-of-plane modes. On gold colloids, the relatively strong enhancement of the ring breathing mode (1000 cm^{-1}) in the SERS spectrum compared to the weak normal Raman spectrum suggests that the TNT molecules oriented perpendicularly with respect to the particle surface. Also, the signal amplification factor in gold (10^5) was better than that of silver (10^2).

Hainer Wackerbarth and co-workers [6] developed an explosives detection principle based on SERS to differentiate between explosives and contaminants. The principle of the device was based on cooling of a nanostructured gold surface to adsorb the explosives from a stream of explosives dissolved in acetonitrile. The substrate was cooled to 5 °C. For substrate temperatures below 5 °C, air moisture crystallization occurred which prevented the adsorption of explosive molecules on the surface. A portable and robust detection system was developed by assembling a standard Raman spectrometer, a cooling system and the SERS substrate into a casing. Based on the Nitro modes different explosives were detected. However, the detection technique was limited by the substrate temperature.

Sylvia [7] demonstrated vapor phase detection of 2, 4-DNT at concentration levels of 5 ppb. The SERS substrates were fabricated by gold foil coupons of 0.1 mm thickness. They were first polished and then electrochemically roughened in 0.1 M KCl. The substrates were soaked overnight in distilled water to remove excess chloride ions and were subsequently cleaned. 2, 4-DNT solution was spotted on the substrates and the SERS studies were performed using 785 nm laser coupled to fiber optic Raman probe. This work demonstrated detection of explosives in liquid phase and involved a complicated substrate preparation technique.

Jerez-Rozo [8] focused on detection of TNT in aqueous solution using metal nanoparticles to produce high sensitivity and molecular specificity. Chemical reduction technique was used to synthesize gold, silver, and Ag/Au colloids with a particle size of 35-80 nm. TNT was detected through an indirect method that involved alkaline hydrolysis of TNT. Out of the different methods of nanoparticle synthesis suggested here, silver colloids prepared with citrate as reducing agent offered the best enhancement and TNT was detected. Previous works on SERS of explosives were limited to either solution or powder samples and the results were limited and not conclusive.

In the present work, we detect explosives in the vapor phase using SERS for the first time. Vapor phase detection of explosives was difficult in the past because of the low vapor pressure of the analyte and photochemical decomposition under Raman laser. The SERS substrate employed in the present work was fabricated by a vacuum deposition step followed by solution immersion and therefore it is scalable. The details of substrate fabrication are mentioned in Chapter 3.

CHAPTER 3

METHODOLOGY

3.1 Overview

This chapter presents the details on the methodology employed to fabricate reproducible ‘nanometal-on-semiconductor’ SERS substrates. It also discloses the measurement conditions and protocols to detect TNT vapor.

3.2 Silicon thin film deposition

The silicon films were deposited on 3" × 3" Corning 1737 code glass slides. The glass slides were cleaned in order to remove all particles and organic residues from the surface. These slides were immersed in 50% IPA solution (Isopropyl Alcohol) (125 ml of 99% IPA+ 125 ml of DI water) and the glass surface was scrubbed with a brush to get rid of the organic residues and adsorbed impurities. Subsequently, ultrasonication in 50% IPA solution was carried out for 10 minutes. The slides were then rinsed in DI (deionized) water and ultrasonicated for 5 minutes to remove the IPA residue. The glass

slides were then removed from the ultrasonicator and blow dried using argon gas. The clean glass slides were sent to Penn State Nanofabrication Facility for silicon thin film deposition using Plasma-enhanced Chemical Vapor Deposition (PECVD) technique. The deposition was performed at a temperature of 120 ºC and power of 100 W. 12 sccm SiH_4 and 250 sccm H_2 mixture was employed as the precursor gas at a process pressure of 5 torr. The deposition was carried out for 10 s to obtain a film thickness of 20 nm.

3.3 Analyte

The TNT simulant was purchased from XM division of Van Aken International. The NESTT (Non- hazardous Explosive for Security Training and Testing) TNT was in the form of fused silica coated with TNT. Other explosives namely 2, 4 DNT (Dinitrotoluene); 2, 6 DNT (Dinitrotoluene); 1, 3, 5 TNB (Trinitrobenzene); 1, 3 DNB (Dinitrobenzene); NB (Nitrobenzene) 2-NT (Nitrotoluene) and 4-NT (Nitrotoluene) used in the present work were purchased from Sigma-Aldrich.

3.4 Nanoparticle synthesis

Silicon films deposited on glass were cut into 10 mm × 8 mm samples to accommodate them inside the optical cell. The reduction process in preparation of SERS-active substrates is illustrated in Fig. 3.1.

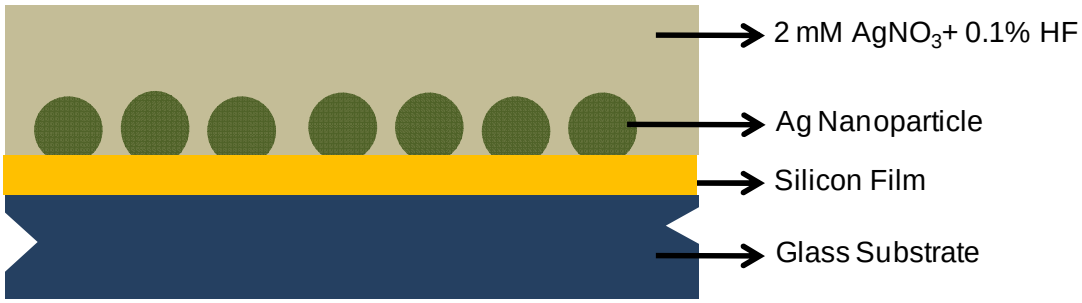

Figure 3.1. Synthesis of silver nanoparticles on silicon film.

The silver nanoparticles were synthesized by immersion of the Si-coated substrate for 30 s in a metal salt solution consisting of 2 mM $AgNO_3$ and 0.1% HF. The silicon film reduces Ag^+ ions to form Ag nanoparticles on the surface and immobilizes the nanoparticles. This electroless reduction process produces clean and surfactant-free nanoparticles [9]. Charge transfer occurs between silicon and silver due to Fermi level difference as a result of which opposite charging occurs between silver and silicon. This opposite charging helps the silver nanoparticles to be anchored to the silicon film without the need of a binding agent. Also, due to same charge polarity, repulsion occurs between the silver nanoparticles preventing their coalescence despite a few nm interparticle spacing. Hence, pronounced plasmon hybridization and high enhancement factor SERS substrates are obtained through this novel nanoparticle synthesis technique. HF present in the solution continuously etches away silicon oxide formed during the redox reaction which would otherwise impede silver's nucleation. Reduction reaction on the silicon surface is stopped by immersing the substrate in DI water.

3.5 Exposing the nanoparticles to TNT vapor

The TNT analyte was wrapped in a small piece of lab-grade wiper and placed inside a septum-sealed optical cell. The SERS substrate was enclosed in the same cell without any contact with TNT as shown in Fig. 3.2.

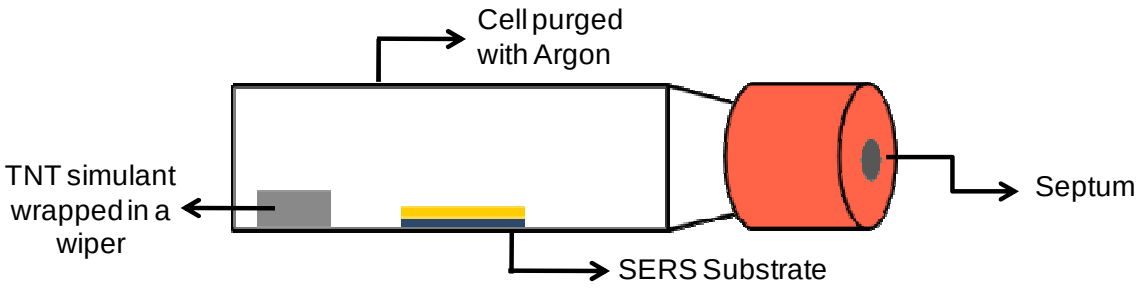

Figure 3.2. Schematic representation of the SERS substrate inside the optical cell.

The optical cell was then purged with argon gas. The experimental set up for purging the optical cell is shown in Fig. 3.3. Two needles were pierced into the septum of the optical cell, one for gas intake and the other for gas exit. The inlet needle was connected to the argon gas cylinder and the outlet needle was left open to air.

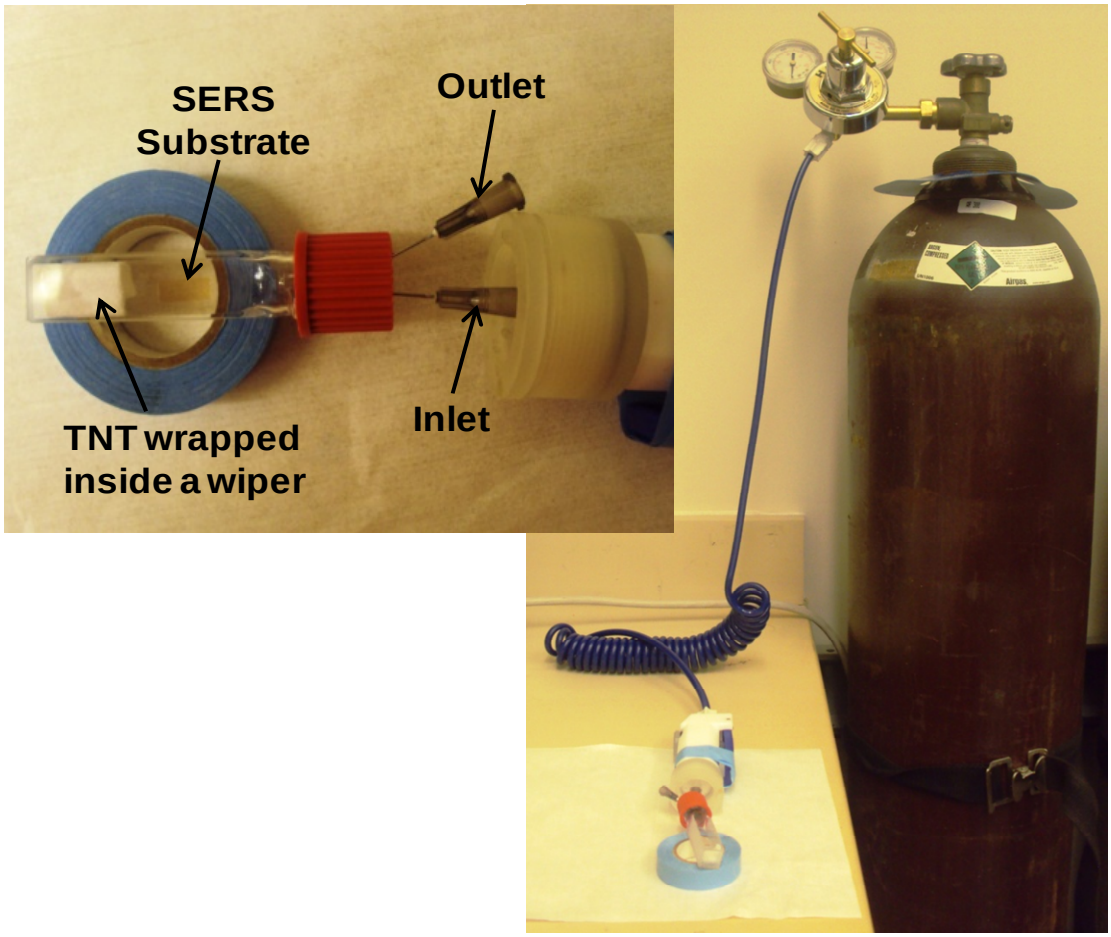

Figure 3.3. Experimental set up for purging the optical cell.

Gas inlet pressure was regulated to 1 psi above atmosphere allowing the flow of argon gas into the cell. After purging the cell for 10 minutes, the outlet needle was first removed, followed by the inlet needle. Subsequently, the optical cell was ensured to be at atmospheric pressure by using a needle connected to a syringe. The sample was left undisturbed overnight for TNT to reach solid-vapor thermodynamic equilibrium.

3.6 SERS Acquisitions

SERS acquisitions were performed using a Renishaw RM 1000 confocal micro-Raman spectrometer, equipped with 1800 l/mm grating and a thermoelectric cooled CCD detector. The substrate was excited with a Spectra-Physics 160 series 514 nm Ar^{+} ion laser at an incident power of 2.5 mW. The Raman spectrometer was coupled with a Leica DMLM microscope and the signal was collected using an objective lens of 20× with 0.4 numerical aperture and a working distance of 12 mm. The laser probe was defocused by 100% as controlled by the Wire 2.0 interface software setting the laser spot size to 64 µm. The SERS spectrum was centered at 1200 cm^{-1} and collected in the range of 700-1700 cm^{-1} with an integration time of 10 s. Figure 3 shows the graphical illustration of SERS acquisition.

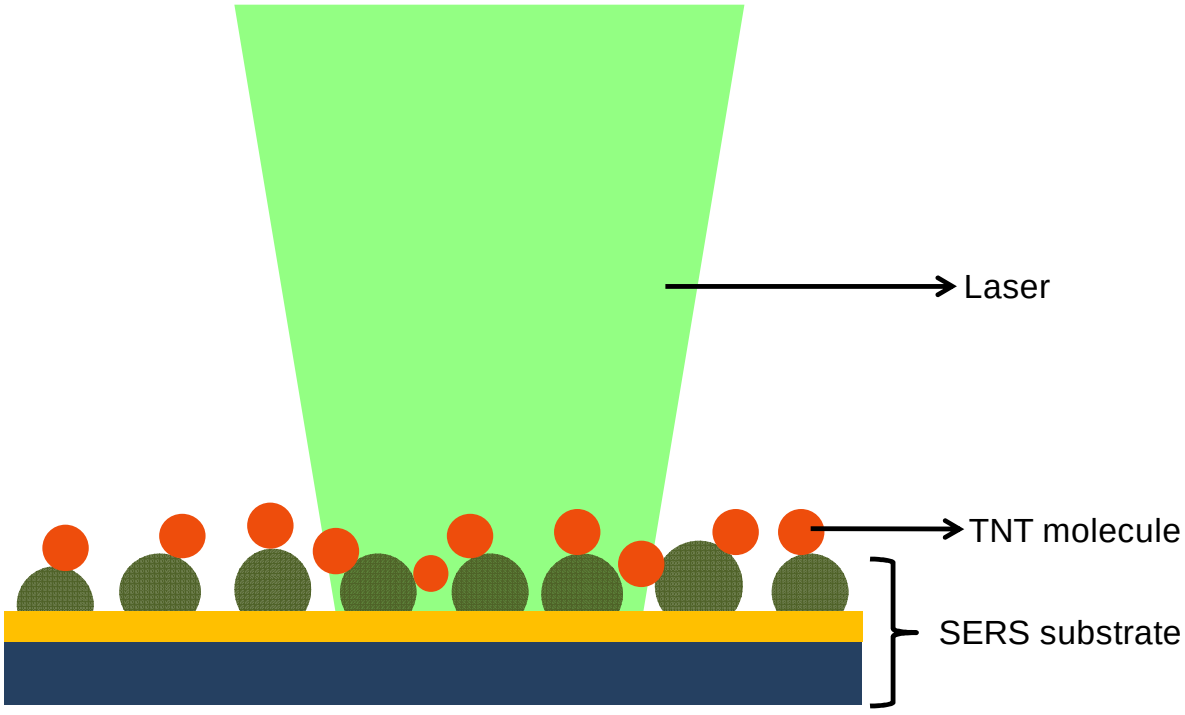

Figure 3.4. Graphical illustration of SERS acquisition.

3.7 Nanoparticle temperature measurement using Raman Spectroscopy

The temperature of the nanoparticles under the conditions of SERS acquisition was measured using the Raman scattering. For a given vibrational mode, the ratio of anti-Stokes Raman scattering to the Stokes Raman scattering is the Boltzmann factor:

$$\frac{I_{as}}{I_s} = e^{-E_p / kT} \qquad 3.1$$

where,

I_{as} = Anti-stokes Raman Intensity

I_s = Stokes Raman Intensity

E_P = Phonon energy (i.e., Raman shift)

k = Boltzmann constant (8.617×10^{-5} eVK^{-1})

T = Temperature (K)

The phonon energy (E_p) is calculated using the relation,

$$E_p = \frac{hc}{\lambda} \qquad 3.2$$

where,

hc = 1.24 eV µm (h is Planck's constant and c is speed of light)

$1/\lambda$ = wavenumber of Raman peak

In the present work, the temperature of the silver nanoparticles was calculated using the Stokes and Anti-Stokes Raman peaks of FBT (4-flouorbenzenethiol) molecules adsorbed on Ag nanoparticles. The Raman measurements were performed on WiTec alpha 300R system. A 532 nm Nd:YAG (neodymium-doped yttrium aluminium garnet)

laser was used as an excitation source. A grating of 600 g/mm and an objective lens of 20× was employed for collecting the signal. The Stokes and anti-Stokes peaks were measured simultaneously and produced significantly sharp peaks with high signal to noise ratio as will be disclosed in Chapter 4.

CHAPTER 4

RESULTS AND DISCUSSION

4.1 Overview

This Chapter presents SERS of TNT in the vapor phase acquired using the substrate approach of the present thesis. The “nanometal-on-semiconductor” SERS substrates employed in the present work are characterized by Atomic Force Microscopy (AFM) and optical absorption spectroscopy. The SERS spectrum of TNT vapor is compared with the Raman of TNT simulant and frequency shifts in the vibrational modes of TNT are observed due to SERS effects. SERS spectrum of TNT vapor is monitored for extended time and the kinetics of different peaks are analyzed. It is observed that each peak follows a different kinetics scale indicating different adsorption configurations or sites of TNT on the silver nanoparticle surface. Three different adsorption configurations of TNT have been identified. To further study the kinetics of these peaks, SERS of TNT is carried out in ambient air. Also, the temperature of the nanoparticles under Raman laser is calculated using the ratio of Stokes to anti-Stokes scattering. This chapter also

presents the vapor phase detection of other explosives such as RDX and PETN using the same SERS substrate.

4.2 Physical Characterization of SERS substrates

4.2.1 Atomic Force Microscopy

The nanometal-on-semiconductor SERS substrates were fabricated using the method described in Chapter 3. The nanoparticles were synthesized by immersion of the PECVD deposited silicon film in 2mM $AgNO_3$ + 0.1% HF solution for 30 s. The silver nanoparticles were characterized using a Dimension V SPM (Veeco) atomic force microscope operated at tapping mode with silicon cantilever of nominal resonance frequency of 160 kHz (MicroMasch USA). Figure 4.1 shows the AFM image of the SERS substrate, provided by Dr. Susheng Tan from NanoScale Fabrication and Characterization Facility at the University of Pittsburgh.

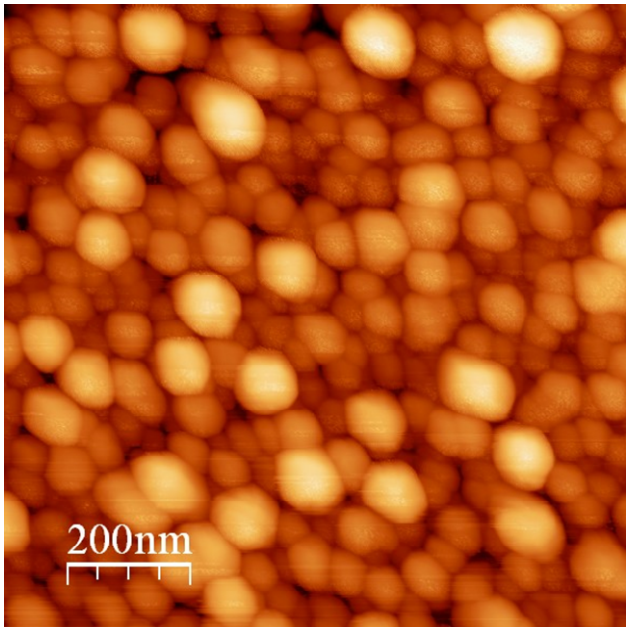

Figure 4.1. Representative AFM image of the Ag nanoparticles on the SERS substrate.

The Ag nanoparticle size distribution is calculated with the help of software called ImageJ and is 75 ± 18.5 nm. From the AFM image we also infer that the average nanoparticle separation is only a few nm.

4.2.2 UV-Visible Spectroscopy

The silver nanoparticles were also characterized using a double-beam Cary 300 Bio UV-Vis spectrophotometer. The optical extinction of the silver nanoparticles reduced on silicon film was measured. In optical spectroscopy, extinction (E) is defined as

$$E = -\log(T) \qquad 4.1$$

where T is the transmission measured by a spectrophotometer. It is the measure of how intense a medium absorbs + scatters light. The extinction of the silver nanoparticles was obtained from the difference

$$E_{sample} - E_{reference}$$

where,

sample = silver nanoparticles + residual silicon + glass substrate + optical cell,

reference = glass substrate+ optical cell.

A plane glass substrate was used as a reference instead of a silicon film, because majority of the silicon film was consumed during the electroless deposition of silver nanoparticles. The optical extinction was acquired from 200 to 800 nm at a scan rate of 600 nm/min. The optical extinction was acquired for two reasons: i) to study the localized

surface-plasmon resonance in the silver nanoparticles; ii) to monitor the reproducibility of the SERS substrates. The extinction spectrum of the nanoparticles is shown in Fig. 4.2.

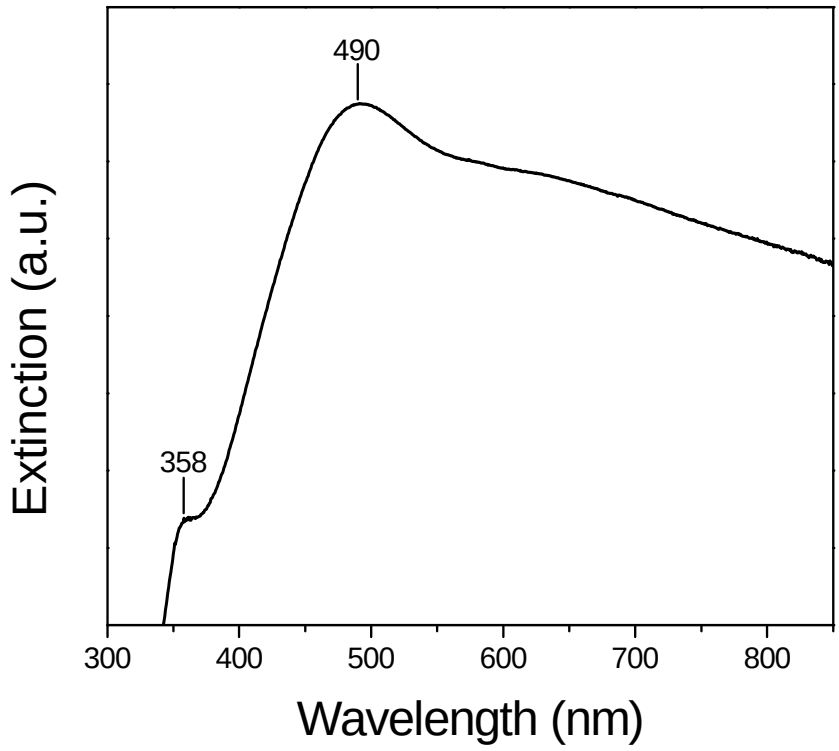

Figure 4.2. Extinction spectrum of Ag nanoparticles on Si film synthesized by immersion in 2 mM $AgNO_3$ + 0.1 % HF for 30 s.

In Fig. 4.2, the 358 and 490 nm peaks are associated with quadrupole and dipole plasmon resonance modes, respectively. The hump beyond the 490 nm band is attributed to hybrid plasmon mode due to strong electromagnetic interaction between closely placed nanoparticles (i.e. the interparticle spacing is less than the diameter of the nanoparticles) [59].

4.3 SERS of TNT vapor and Raman of TNT simulant

Figure 4.3 compares the SERS of TNT vapor and Raman scattering of TNT. The Raman spectrum was acquired directly from the simulant. The Raman acquisitions were performed using a Renishaw RM 1000 micro-Raman spectrometer. A 514 nm Ar^+ ion laser at an incident power of 3.7 mW was used. The Raman signal was collected using a 20× objective lens with 0.4 numerical aperture and working distance of 12 mm. The predominant Raman peaks of TNT obtained from TNT simulant given in Table 4.1 are in accordance with the literature [11, 23, 61, 63].

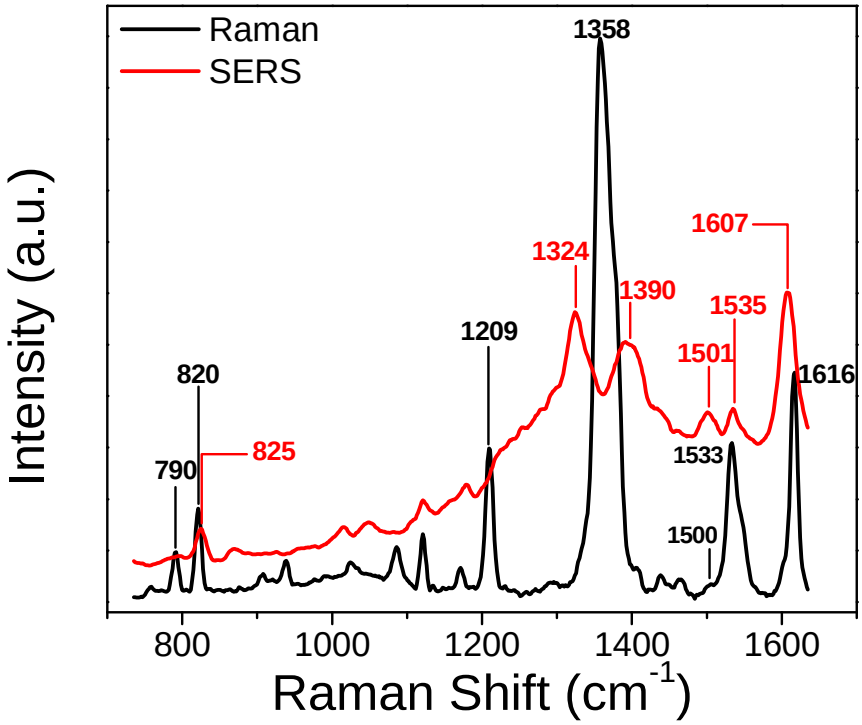

Figure 4.3. SERS of TNT vapor and Raman scattering of TNT simulant.

In SERS, frequency shifts in the vibrational modes are observed as seen in Fig 4.3. These shifts are attributed to the electron transfer between TNT and Ag nanoparticles. Chemisorption to the metal surface modifies the electron density distribution over the adsorbate molecule leading to changes in the bond stiffnesses and

thereby vibrational frequencies. Also, charge transfer between metal orbitals and adsorbate orbitals may cause a change in the polarizabilty of the adsorbate resulting in the observation of new peaks [64].

Table 4.1. Raman peaks for TNT and their designation [11, 23, 61, 63].

Raman Shift (cm^{-1})	**Vibrational Mode**
790	C–H out-of-plane bending
820	NO_2 scissoring
1209	C_6H_2–C vibration
1358	NO_2 symmetric stretching
1533	NO_2 asymmetric stretching
1616	C═C aromatic stretching vibration

4.4 Different adsorption configurations of TNT

The 1358 cm^{-1} peak in the Raman spectrum of TNT as seen in Fig 4.3 is associated with symmetric nitro-stretching mode. This peak splits into two modes: 1324 and 1390 cm^{-1} as seen in the SERS spectrum. Splitting of a vibrational mode of a molecule is possible due to several reasons, such as adsorption of the molecule on different crystal planes of the nanoparticle, defragmentation of the molecule into two or more different species, or different adsorption configurations of the molecule on the nanoparticle surface.

In the present work, we conclude that the splitting in the nitro-stretching mode has not occurred due to adsorption of TNT on different crystal planes of silver. If different

crystal planes caused the splitting of the nitro-stretching mode, a similar splitting would be observed for other peaks. From the SERS spectrum of TNT in Fig 4.3, it is observed that no splitting occurs for atleast the majority of peaks.

An alternative explanation for the splitting of 1358 cm^{-1} Raman peak into two SERS peaks is the defragmentation of TNT into two or more species. The most possible fragments of TNT are 2, 4 DNT, 2, 6 DNT, 1, 3, 5 TNB, 1, 3 DNB, 2-NT, 4- NT, NB, toluene, and benzene. SERS acquisitions for each of these fragments were performed in vapor phase using the SERS substrates and under the same conditions. SERS acquisitions were performed using Renishaw RM 1000 confocal micro-Raman spectrometer at 2.5 mW incident power and 10 s signal integration time. Fig. 4.4 shows the SERS spectra of the most possible fragments of TNT mentioned above. However, none of these fragments yield the same SERS peaks as that of TNT. Hence, it is more likely that the two SERS peaks are associated with different adsorption configurations and not defragmentation of TNT.

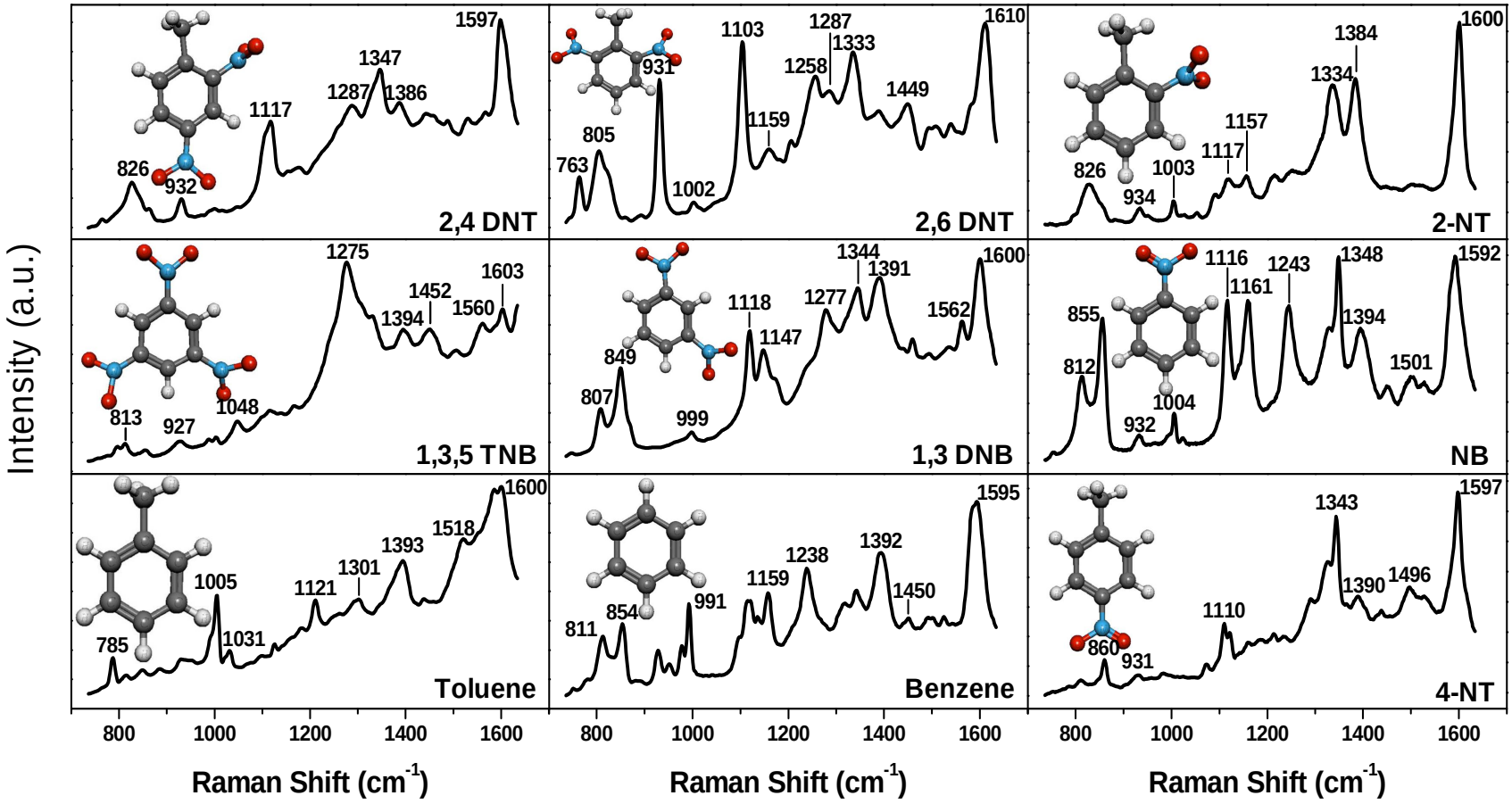

Figure 4.4. SERS spectra of all possible fragments of TNT.

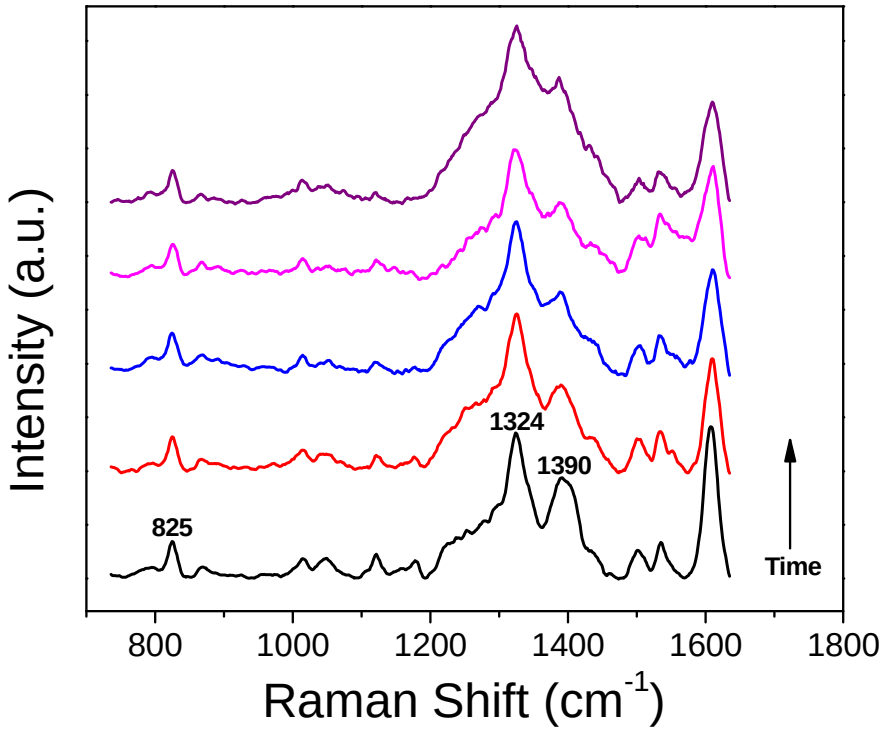

Figure 4.5. Time series spectra of TNT captured for the first 50 s in 11 s intervals.

To investigate different adsorption configurations, SERS of TNT is monitored for 50 s in 11 s intervals (10 s integration time + 1 s readout) and the spectrum evolves as seen in Fig. 4.5. It is observed that the kinetics of 1324 and 1390 cm^{-1} peaks follow different time scales indicative of different populations of TNT. Since the nitro-stretching is in plane, and the surface-enhanced field is perpendicular to the silver surface, 1324 and 1390 cm^{-1} peaks must be associated with the "standing-up" configuration as illustrated in Fig. 4.6a and 4.6b. One configuration is due to adsorption of TNT on the silver nanoparticle with the 2 or 6- nitro group close to the methyl group and the second configuration arises from adsorption of the 4-nitro-group opposite to the methyl group. As seen in Fig. 4.5, the 1324 cm^{-1} peak persists for longer duration while the 1390 cm^{-1} peak disappears faster that we attribute to its higher instability due to the steric hindrance caused by the methyl group between Ag surface and TNT as depicted in Fig 4.6b.

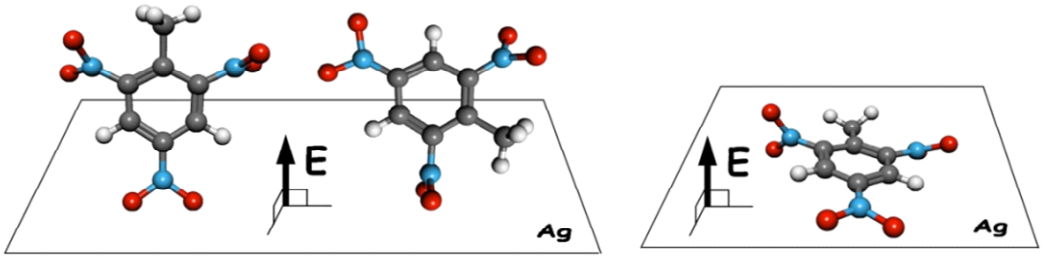

Figure 4.6. TNT molecules adsorbed to Ag in "standing up" and "lying down" configurations.

SERS of TNT is further monitored for longer times (e.g., 400 s). It is observed that the 825 cm^{-1} peak exhibits the slowest kinetics as illustrated in Fig. 4.7. This mode is ascribed to the "out-of-plane" vibrations of the nitro groups, suggesting that it must be associated with the "lying-down" configuration as illustrated in Fig. 4.6c. The lying-down configuration should possess the highest stability as multiple nitro groups can undergo bonding with the silver surface at the same time. This deduction is consistent with the slowest disappearance of this peak as seen in Fig. 4.7. Further, the slow kinetics of the 825 cm^{-1} peak may not be due to desorption, and it may actually arise from decomposition of TNT. Indeed, the systematic increase of SERS background in Fig. 4.7 is indicative of a photoproduct.

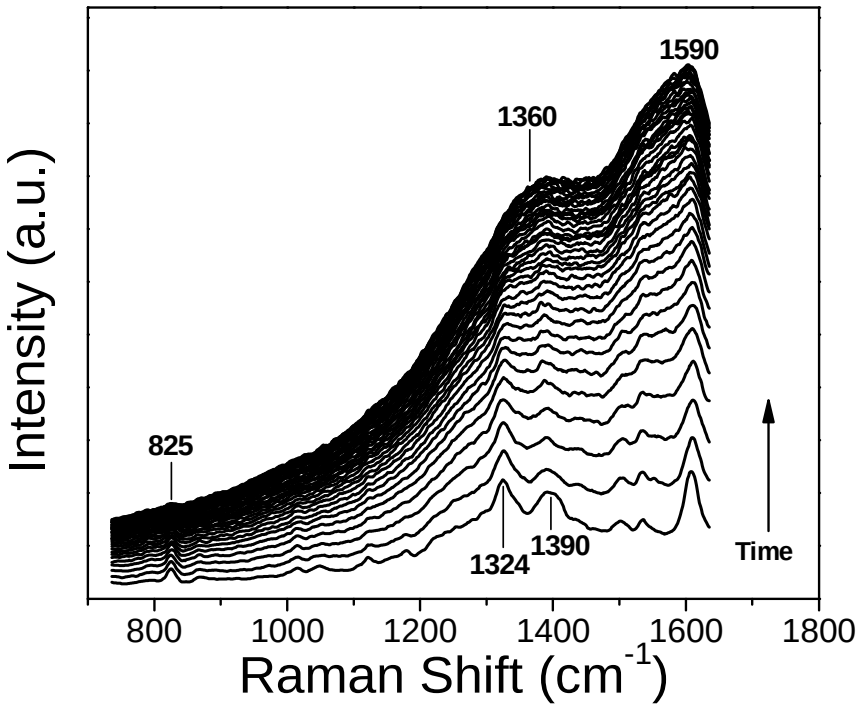

Figure 4.7. Time series SERS spectra of TNT captured at intervals of 11 s.

This photoproduct or background formed due to decomposition of TNT is quantified choosing the SERS intensity at 1360 cm^{-1} as seen in Fig. 4.8. The SERS spectra is further monitored for 1200 s. The normalized intensities of 825 cm^{-1} and 1360 cm^{-1} peaks are calculated using the following equations

$$\frac{I_{825,t=0} - I_{825,t}}{I_{825,t=0}} \qquad 4.2$$

$$\frac{I_{1360,t}}{I_{1360,t=1200}} \qquad 4.3$$

where $I_{825,t}$ represents the intensity of the 825 cm^{-1} peak at time 't', $I_{1360,t}$ represents the intensity of the 1360 cm^{-1} peak at time 't'. The normalized intensity reduction of the 825 cm^{-1} peak is also illustrated in Fig. 4.8. The "intensity reduction of the 825 cm^{-1} peak"

has notable agreement with the "intensity increase of the 1360 cm^{-1} band," which is characteristic of sp^3 carbon, as illustrated in Fig. 4.8. Therefore, the increasing SERS background is correlated with the decomposition of lying-down TNT according to the reaction:

$$2\ C_7H_5N_3O_6 \rightarrow 3\ N_2 + 5\ H_2O + 7\ CO + 7\ C$$

Transformation of TNT to solid carbon is also evident from the increasing background peaking at ~1590 cm^{-1}, which is indicative of sp^2 carbon.

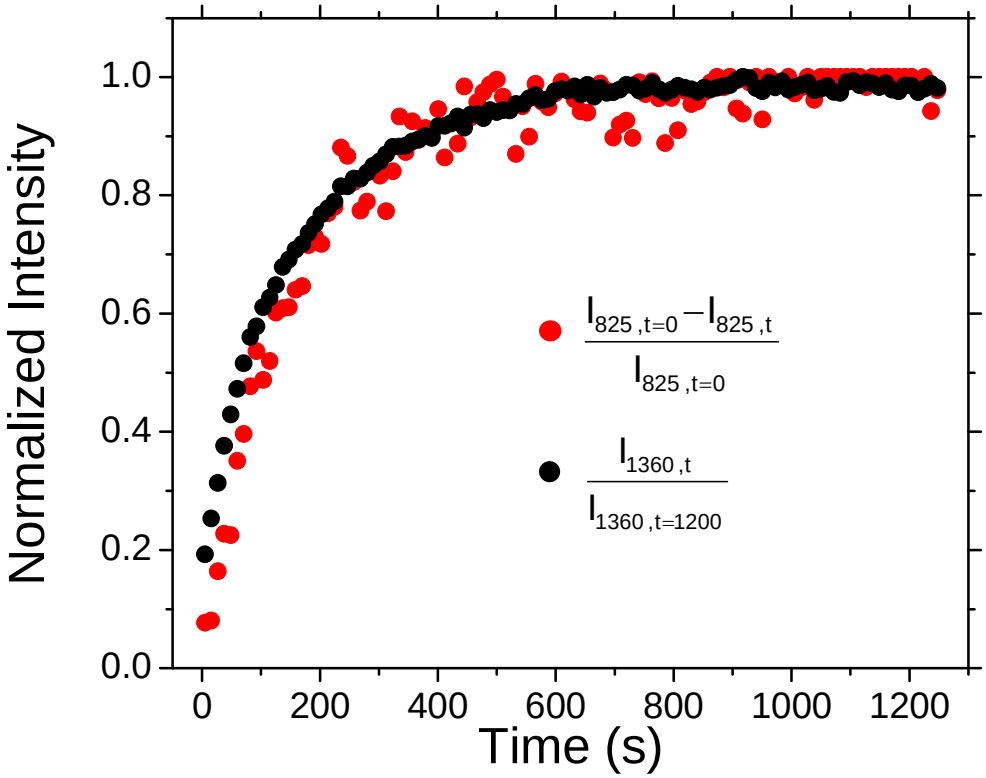

Figure 4.8. Normalized intensity increase of the SERS baseline (adopted as 1360 cm^{-1}) and normalized intensity reduction of the 825 cm^{-1} peak as a function of time. Series correspond to 11 s intervals.

4.5 Temperature of silver nanoparticles

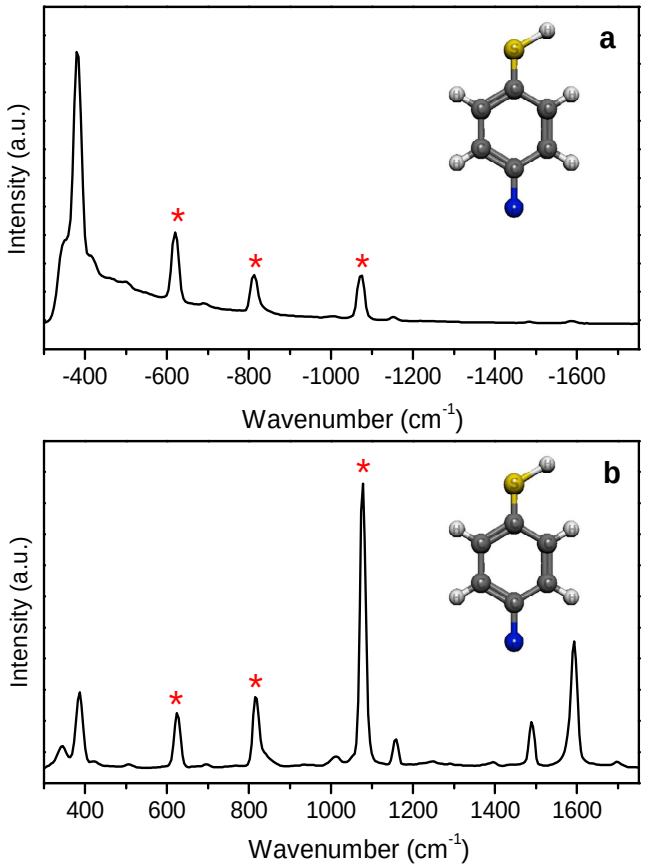

Figure 4.9. (a) Anti-Stokes and (b) Stokes Raman scattering spectra of FBT.

To elucidate laser-induced decomposition of TNT, temperature of the silver nanoparticles was calculated from the Boltzmann factor of FBT molecules using Raman spectroscopy as discussed in Section 3.7. The Stokes and anti-Stokes Raman scattering spectra of FBT used for the temperature measurement are shown in Fig. 4.9. Stokes and anti-Stokes Raman peaks at 621, 814, and 1074 cm^{-1} were used for temperature calculation. The nanoparticle temperature was calculated as 27 °C (close to room temperature) under the conditions of SERS acquisitions. This temperature is significantly below TNT's detonation temperature of 333 ºC [65]. The temperature of the nanoparticles being very close to ambient temperature under the SERS conditions

suggests that no laser-induced heating occurs during SERS acquisition and the laser-induced decomposition of TNT is a photochemical effect rather than a photothermal effect.

4.6 SERS of TNT in ambient air

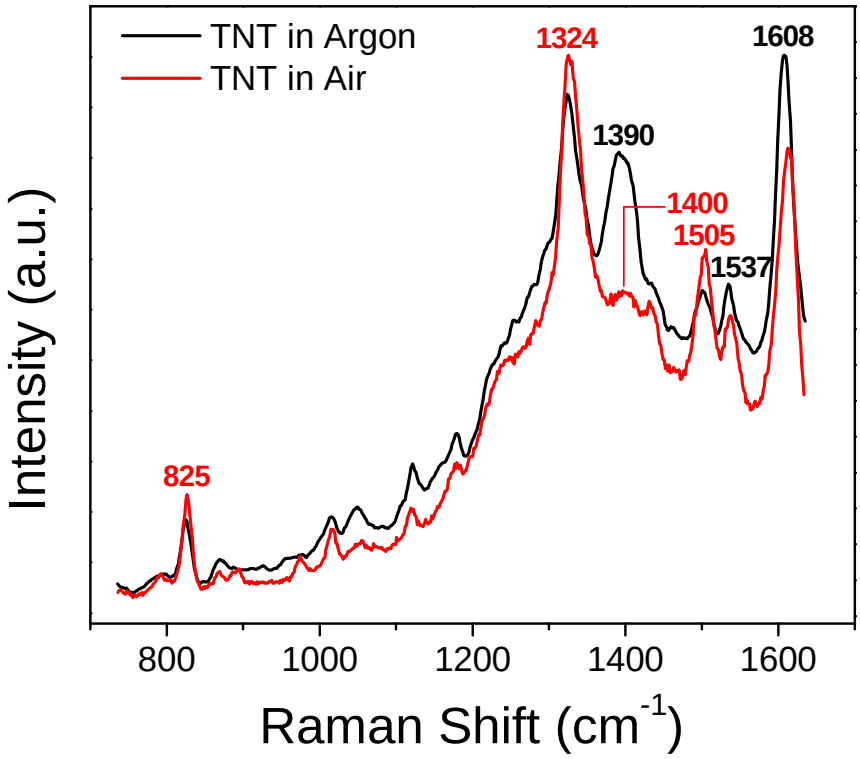

Figure 4.10. SERS spectra of TNT vapor in argon and ambient air.

To elucidate the origin of splitting of the symmetric nitro peaks, SERS acquisitions were further carried out in ambient air. The nanoparticles were exposed to TNT vapor in ambient air and left undisturbed overnight for TNT to reach solid-vapor thermodynamic equilibrium. SERS acquisitions were performed on the substrate and it was observed that in ambient air, the intensity of the ~1390 cm^{-1} peak decreased and the intensity of the 1324 cm^{-1} peak increased as seen in Fig. 4.10. The decrease in the intensity of 1390 cm^{-1} peak is likely due to selective O_2– or H_2O–induced desorption of

the weaker configuration of TNT (associated with the 1390 cm^{-1} peak). However, all the other signature peaks of TNT were observed, validating the SERS substrate for vapor phase detection of TNT in ambient air.

To check if the SERS peak at 1390 cm^{-1} recovers in inert ambient, SERS acquisitions were first performed in ambient air. Subsequently, the same optical cell containing the SERS substrate was purged with argon gas for 10 min. It was observed that the weakly adsorbed TNT configuration associated with 1390 cm^{-1} did not reappear in the argon ambient as seen in Fig. 4.11. This suggests that the O_2– or H_2O–induced desorption of the 1390 cm^{-1} peak is not reversible.

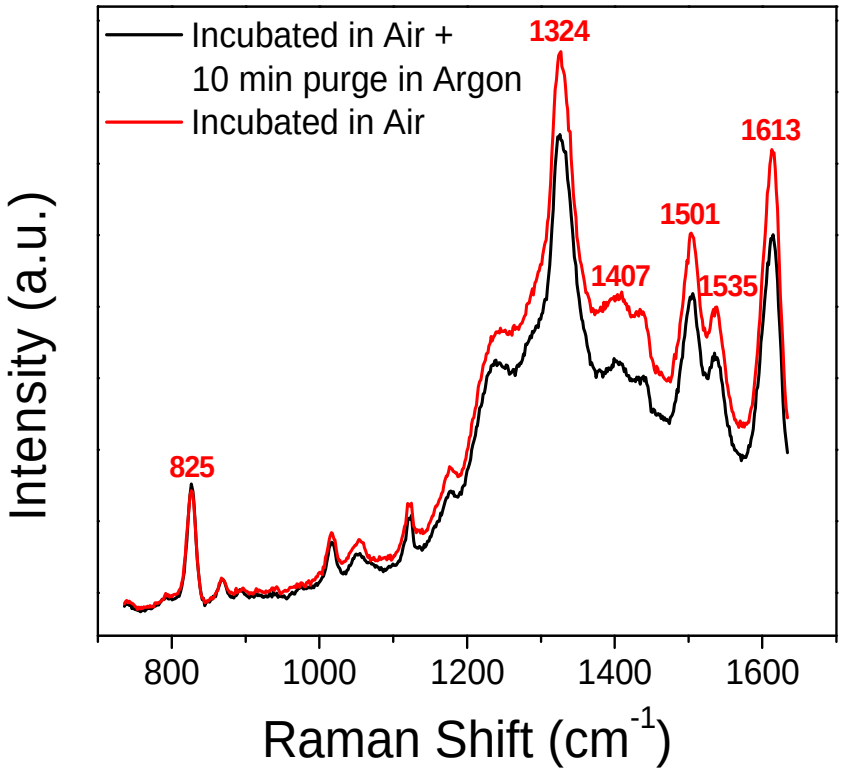

Figure 4.11. SERS of TNT in ambient air followed by argon.

4.7 SERS of TNT in pure oxygen environment

To check if the decrease in the intensity of the SERS peak at ~1390 cm^{-1} associated with the weaker configuration of TNT is due to its selective O_2–induced desorption, SERS of TNT was acquired in pure oxygen. The SERS substrate and TNT were enclosed in an optical cell without any contact. The optical cell was purged with oxygen gas for 10 min. Ultra high purity compressed oxygen gas cylinder was purchased from Stillwater Steel supply. The SERS substrate was left undisturbed overnight for TNT to reach solid-vapor thermodynamic equilibrium. Figure 4.12 shows the SERS spectrum of TNT in oxygen environment.

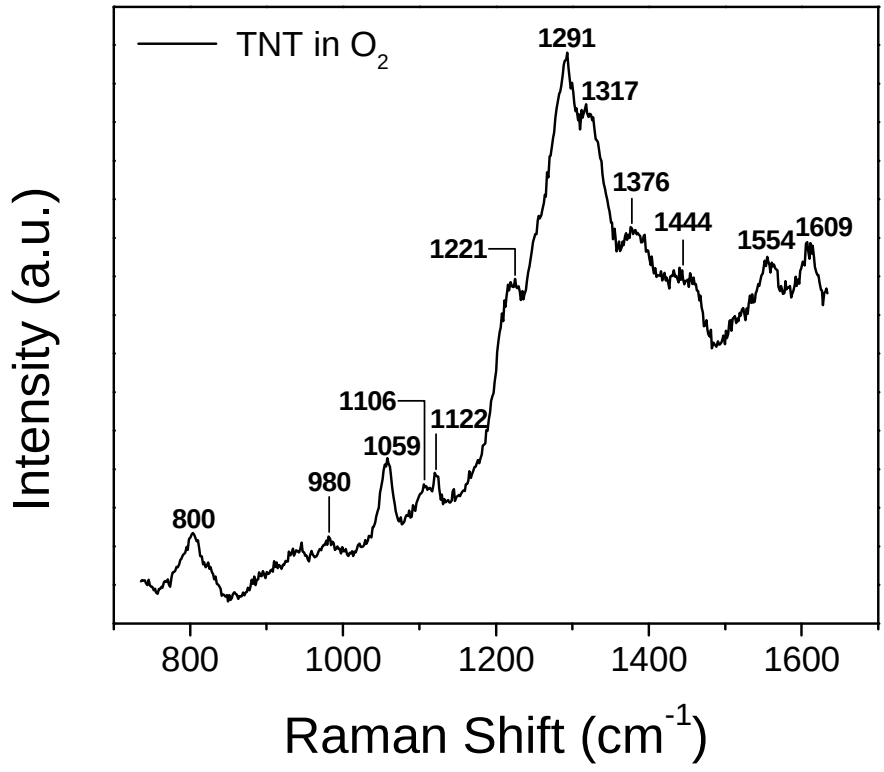

Figure 4.12. SERS spectrum of TNT in O_2 environment.

In pure oxygen, a new peak at 1291 cm^{-1} was observed as seen in Fig. 4.12. Moreover, two peaks were observed at 1317 and 1376 cm^{-1} similar to 1324 and 1390 cm^{-1} peaks in argon environment. The out-of-plane bending mode of TNT was observed at 800 cm^{-1}. It is likely that TNT in the optical cell reacts with pure O_2 to produce 1, 3, 5 TNB [66]. Figure 4.13 shows the SERS spectra of 1, 3, 5 TNB in argon and TNT in oxygen environment.

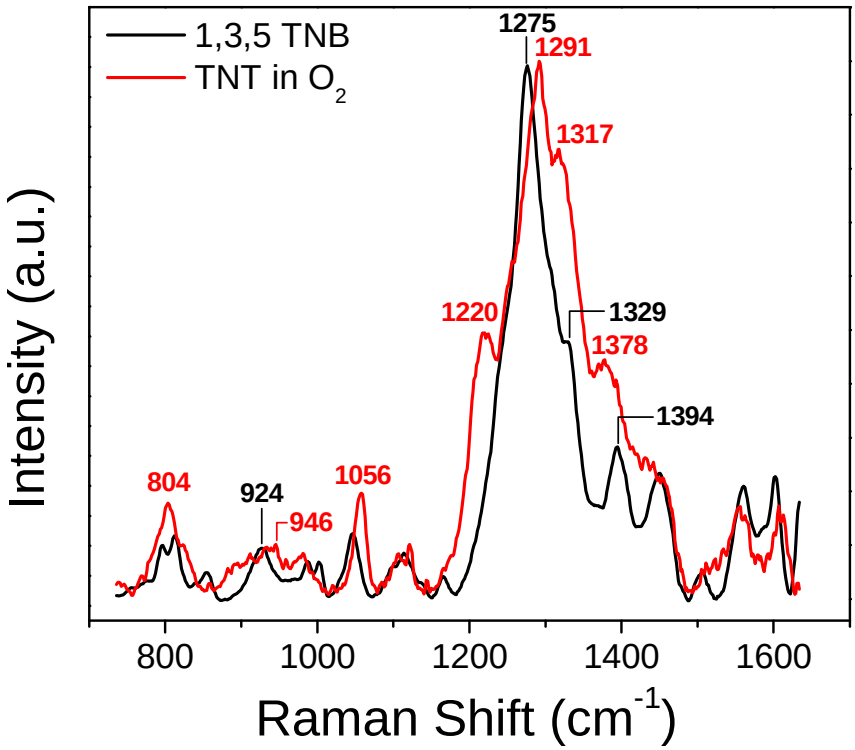

Figure 4.13. SERS spectra of TNT in O_2 and 1, 3, 5 TNB in argon.

4.8 Effect of water vapor on SERS of TNT

SERS of TNT was also acquired in the presence of water vapor. SERS substrate and TNT simulant were enclosed into an optical cell. A small lab-grade wiper wetted with a droplet of water was introduced into the optical cell. Subsequently, the cell was purged with argon gas for 10 min and then left undisturbed overnight. The substrate was

excited with a 514 Ar^+ laser at an incident power of 0.47 mW. The SERS signal was collected using a 20× objective lens with an integration time of 10 s. SERS spectrum of TNT acquired in the presence of 100% relative humidity is shown in Fig. 4.14. A strong peak was observed at 1369 cm^{-1} as seen in Fig .4.14 similar to the 1358 cm^{-1} peak observed in the Raman spectrum of TNT. The presence of water molecules may have prevented the adsorption of TNT to silver nanoparticles. The author believes that TNT molecules do not directly adsorb on the substrate due to the formation of a monolayer of water molecules on the surface. Hence, symmetric nitro-stretching mode is observed at the same frequency as bulk TNT with Raman spectroscopy.

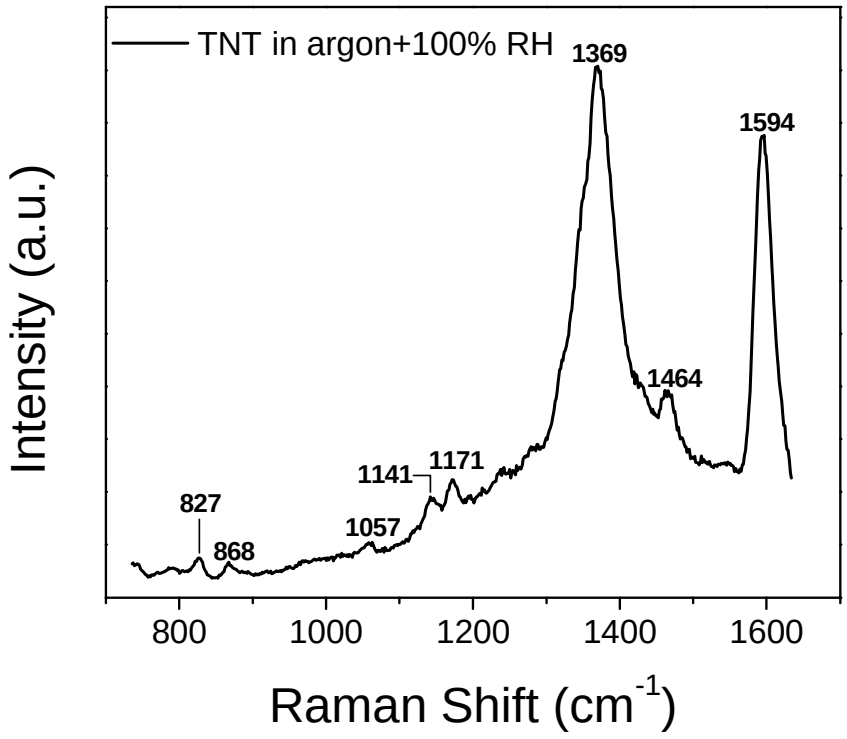

Figure 4.14. SERS of TNT in Ar and 100% RH.

4.9 SERS of TNT in the presence of 20% RH argon

Further, SERS of TNT vapor was acquired with substrates incubated with the TNT simulant in 20% RH argon for 8 h. 100% RH argon (i.e., argon in equilibrium with liquid water and water vapor) was created in another optical cell and a syringe was used to inject 1 ml of 100% RH argon into the argon purged optical cell containing TNT simulant and the SERS substrate. Prior to the injection, 1 ml of dry argon gas was removed from the cell. It was ensured that the cell was maintained at atmospheric pressure. Figure 4.15 shows the SERS spectrum of TNT in the presence of 20% RH argon. It was observed that the weaker configuration of TNT associated with ~1390 cm^{-1} peak reduced in intensity, same as in the case of TNT in ambient air. This suggests that in air H_2O–induced desorption of the weaker configuration of TNT occurs.

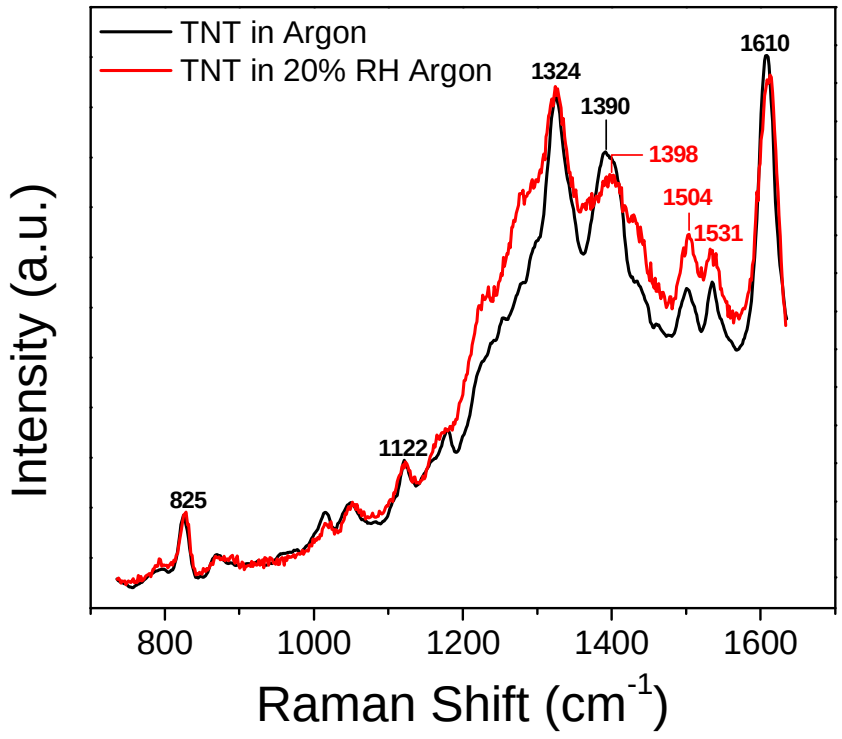

Figure 4.15. SERS of TNT in the presence of 20% RH argon.

4.10 SERS of TNT in dry air

SERS of TNT was further acquired in dry air ambient. A desiccant was used to absorb the water vapor inside the optical cell containing TNT and the SERS substrate. Figure 2 shows the SERS of TNT in dry air ambient. It is observed that the ~1390 cm^{-1} peak appears in the spectrum same as in the case of TNT in argon ambient. This proves that desorption or decomposition of the weaker configuration of TNT associated with the ~1390 cm^{-1} peak is H_2O–induced and not O_2–induced.

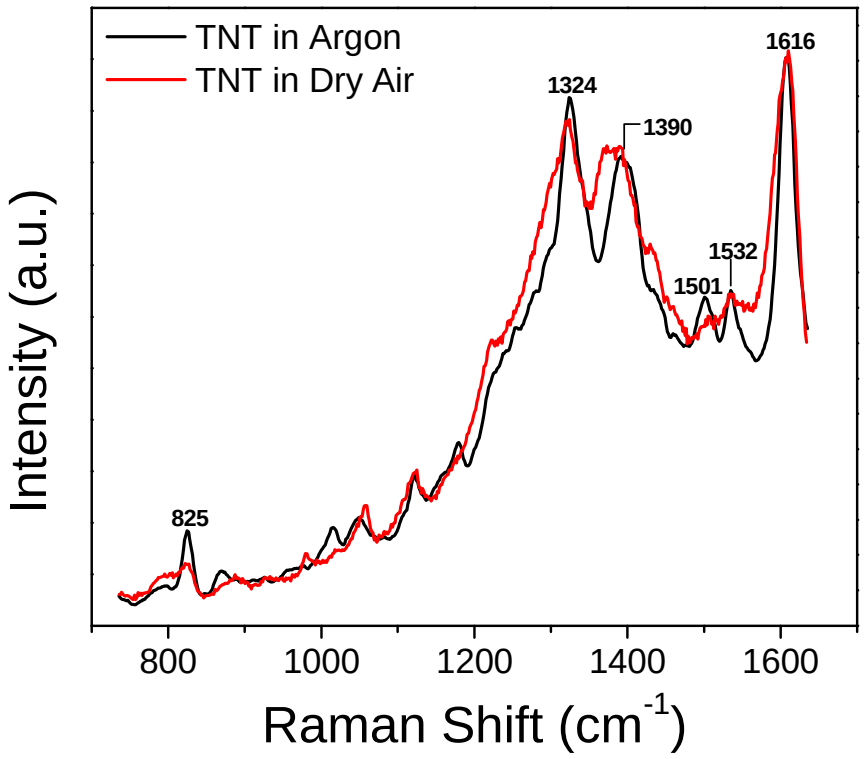

Figure 4.16. SERS of TNT in dry air ambient.

4.11 Vapor phase detection of RDX and PETN

In addition to TNT, the present work also demonstrates vapor phase detection of RDX and PETN as shown in Fig. 4.16. The SERS substrates fabricated in the present work can be employed for detection of all the nitro-explosive compounds.

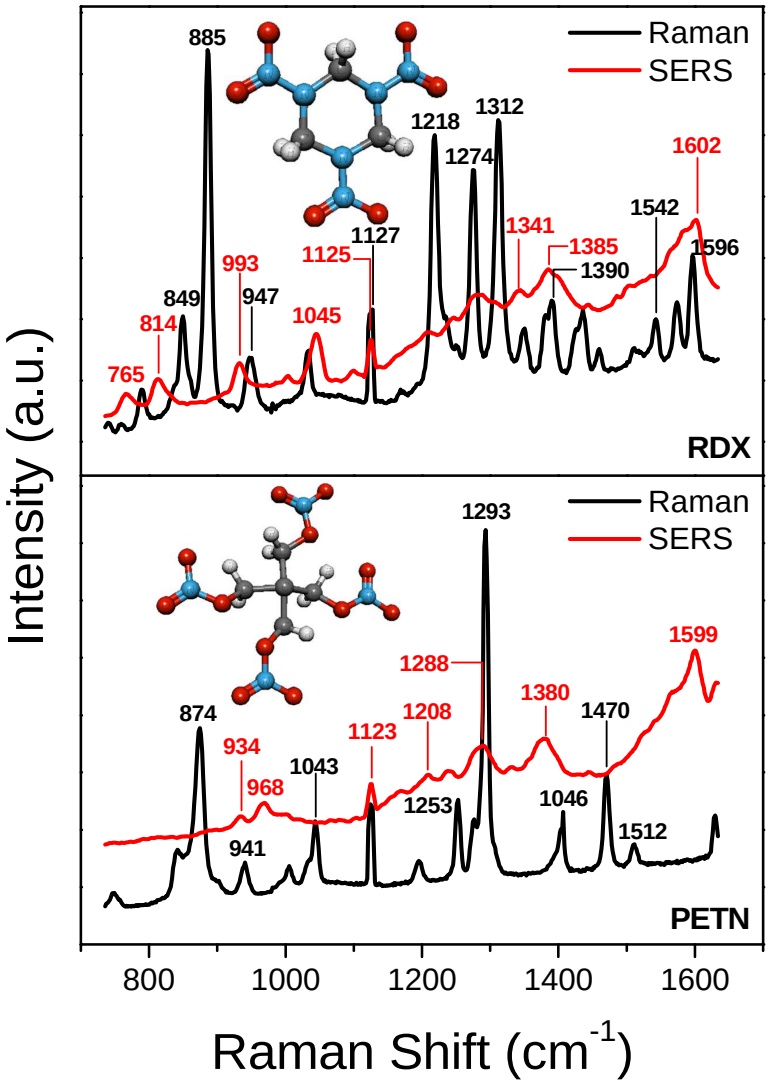

Figure 4.17. SERS and Raman spectra of RDX and PETN.

CHAPTER 5

CONCLUSIONS

Based on the results obtained in this thesis, the following conclusions are drawn:

1) Vapor phase detection of several nitro-explosives is demonstrated using SERS. The "nanometal-on-semiconductor" SERS substrate employed in the present work is fabricated by a vacuum deposition step followed by solution immersion and therefore it is scalable.

2) Despite the transient nature of the SERS spectrum, we show that a reproducible signal is obtained for 10 s signal integration.

3) We gain a clear understanding of the factors, which so far have limited vapor phase SERS of explosives. The three major challenges identified are:

i) low vapor pressure of explosives at room temperature

ii) weak adsorption of the explosives on Ag accounting for laser-induced and/or H_2O–induced desorption

iii) photochemical decomposition of the explosive under Raman laser

4) The present work also suggests different adsorption configurations of TNT on Ag nanoparticles using SERS selection rules. The different configurations are associated with different desorption rates or decomposition rates during the SERS acquisition.

5) Our results indicate that multiple adsorption configurations of an explosive molecule on the nanoparticle surface may complicate the SERS spectrum. In particular, we have verified this possibility for TNT.

6) SERS of TNT and other explosives investigated in this study shows reproducible spectral deviations from Raman scattering. These deviations are attributed to chemisorption-induced electron transfer between the TNT molecule and Ag. Chemisorption to the metal surface modifies the electron density distribution over TNT leading to changes in bond stiffnesses and vibrational frequencies.

7) The nanoparticle surface (i.e., adsorbate) temperature was measured using Raman scattering as 27 °C (close to room temperature) that is significantly below TNT's detonation temperature of 333 ºC. The temperature of the nanoparticle close to ambient temperature suggests that no laser-induced heating occurs and the laser-induced decomposition of TNT is a photochemical effect.

8) In ambient air, weaker configuration of TNT associated with the 1390 cm^{-1} peak disappears. This disappearance is due to selective H_2O–induced desorption of TNT. The configuration associated with the 1390 cm^{-1} peak is not reversible when the ambient is restored to inert from air, with or without the TNT vapor.

9) The SERS substrates fabricated in the present work can be employed for vapor-phase detection of other nitro-explosive compounds.

10) SERS substrate approach employed in this thesis is not practical at the present time, because of the longer incubation time required for TNT to reach solid-vapor equilibrium. However, the SERS substrate can be integrated into a heating chamber and the evaporation rate as well as equilibrium vapor pressure of the explosive residues (i.e., micro- nanoparticles) can be increased. Indeed, this technique is routinely used in conventional IMS detection of the explosives to increase the vapor pressure to ppm levels in a matter of seconds.

BIBLIOGRAPHY

[1] L.C. Shriverclake, K.A. Breslin, P.T. Charles, D.W. Conrad, J.P. Golden, F.S. Ligler, "Detection of TNT in Water Using an Evanescent Wave Fiber-optic Biosensor," *Analytical Chemistry*, vol. 67, p. 2431, 1995.

[2] K.D. Taskiri, J.T. Cronkhite, P.J. Kuan, C. Xing, G. Raghu, J.C. Weissler, R.L. Rosenblatt, J.W. Shay, C.K. Garcia, "Adult-onset pulmonary fibrosis caused by mutations in telomerase," *Proceedings of National Academy of Sciences*, vol. 104, p. 7552, 2007.

[3] D.S. Moore, "Instrumentation for trace detection of high explosives," *Review of Scientific Instruments*, vol. 75, p. 2499, 2004.

[4] S.F. Hallowell, "Screening people for illicit substances: a survey of current Portal technology," *Talanta*, vol. 54, p. 447, 2001.

[5] K. Kneipp, Y. Wang, R.R. Dasari, M.S. Feld, B.D. Gilbert, J. Janni, J.S. Steinfeld, "Near-infrared surface-enhanced Raman scattering of trinitrotoluene on colloidal gold and silver," *Spectrochimica Acta Part A: Molecular and Biomolecular Spectroscopy*, vol. 51, p. 2171, 1995.

[6] H. Wackerbarth, C. Slab, L. Gundrum, M. Niederkruger, K. Christou, W. Viol, "Challenge of false alarms in Nitroaromatic explosive detection- a detection device based on Surface-enhanced Raman Spectroscopy," *Applied Optics*, vol. 49, p. 4367, 2010.

[7] J.M. Sylvia, J.A. Janni, J.D. Klein, K.M. Spencer, “Surface-enhanced Raman Detection of 2,4-Dinitrotoluene Impurity Vapor as a Marker To Locate Landmines,” *Analytical Chemistry*, vol. 72, p. 5834, 2000.

[8] J.I.P Rozo, O.M.P Pedrozo, M.A.B. Cabän, S.P.H Rivera, “Enhanced Raman Scattering of 2, 4, 6 TNT using Metallic Colloids,” *IEEE Sensors Journal*, vol. 8, p. 974, 2008.

[9] K. Bhatt, S. Tan, S. Karumuri, and A.K. Kalkan, “Charge-selective Raman scattering and fluorescence quenching by “Nanometal on semiconductor” substrates,” *Nano Letters*, vol. 10, p. 3880, 2010.

[10] A.K. Kalkan and S.J. Fonash “Laser Activated Surface-Enhanced Raman Scattering Substrates Capable of Single Molecule Detection,” *Applied Physics Letters*, vol. 89, p. 233103, 2006.

[11] I.R. Lewis, N.W. Daniel, and P.R. Griffiths, “Interpretation of Raman Spectra of Nitro-containing Explosive Materials, Part I group frequency and structural class membership,” *Applied Spectroscopy*, vol. 51, p.1854, 1997.

[12] A.M. Farhat, E.A. Bassam, and S.G. James “Chemical Explosives and Propellants,” in *Handbook of Industrial Chemistry -Organic Chemicals*, NY: McGraw-Hill, 2005, p. 458.

[13] G.C. Smith, “The theoretical nitration of Toluene,” in *Trinitrotoluenes and mono and dinitrotoluenes their manufacture and properties*, NY, D. Van. Nostrand Company, 1918, ch. 3, p. 20.

[14] W.C. Roberts and W.R. Hartley, “2,4,6 Trinitrotoluene,” in *Drinking water health advisory: Munitions*, FL, Lewis publishers, 1992, p. 327.

[15] K.S. Ro *et al.*, “Sloubility of 2,4,6-Trinitrotoluene (TNT) in water”, *Journal of Chemical Engineering Data*, vol. 41, p. 758, 1996.

[16] J.M. Phelan, J.L. Barnett, “Solubility of 2,4-Dinitrotoluene and 2,4,6 Trinitrotoluene in water,” *Journal of Chemical Engineering Data*, vol. 46, p. 375, 2001.

[17] Copisarow, *Chemistry News*, vol. 112, p. 247, 1915.

[18] J. P. Agrawal, “Status of explosives,” in *High Energy Materials Propellants, Explosives and Pyrotechnics*, Great Britain, Wiley, 2010,ch. 2, p. 71.

[19] M.B. Pushkarsky, I.G. Dunayevskiy, M. Prasanna, A.G. Tsekoun, R. Go, and C.K.N. Patel, “High-sensitivity detection of TNT,” *Proceedings of the National Academy of Sciences*, vol. 103, p. 19630, 2006.

[20] W.R. Carper, I.P. Davis, and M.W. Extine, “Molecular Structure of 2,4,6-trinitrotoluene,” *Journal of Physical Chemistry*, vol. 86, p. 459, 1982.

[21] N.I. Golovina, A.N. Titkov, A.V. Raevskii, and L.O Atovmyan, “Kinetics and mechanism of phase transition in the crystal of 2,4,6 Trinitrotoluene and Benzotrifuroxane,” *Journal of Solid State Chemistry*, vol. 113, p. 229, 1994.

[22] J.C. Barnes and W. Golnazarins, “The 1:1 Complex of Pyrene with 2,4,6-Trinitrotoluene,” *Acta Crystallographica C*, vol. 43, p. 549, 1987.

[23] J. Clarkson, W.E. Smith, D.N. Batchelder, D.A. Smith, and A.M. Coats, “A Theoretical study of the structure and vibrations of 2,4,6-trinitrotoluene,” *Journal of Molecular Structure*, vol. 684, p. 203, 2003.

[24] C.P. Nash, T.E. Nelson, J.J. Stewart, and W.R. Carper, "Molecular structure and vibrational analysis of 2,4,6-Trinitrotoluene and 2,4,6-Trinitrotoluene-α-d_3," *Spectrochimica Acta*, vol. 45A, p. 585, 1989.

[25] S. Singh and M. Singh, "Explosives detection systems (EDS) for aviation security," *Signal Processing*, vol. 83, p. 31, 2002.

[26] D.M. Sheen, D.L. McMakin, and T.E. Hall, "Three-Dimensional Millimeter-Wave Imaging for Concealed Weapon Detection," *IEEE Transactions On Microwave Theory and Techniques*, vol. 49, p. 1581, 2001.

[27] M.C. Kemp, "Millimeter Wave and Terahertz Technology for the Detection of Concealed Threats – A Review," *Proceedings of SPIE*, vol. 6402, p. 64020D-1.

[28] R.L. Grob and E.F. Barry, "Qualitative and Quantitative Analysis by Gas Chromatography, in *Modern practice of Gas Chromatography*, 4th ed. NJ, John Wiley & Sons, Inc. 2004, ch. 8, p. 404.

[29] P. Nelson, "Index to EPA Test Methods," US EPA New England Region 1 Library, Boston, MA, USA.

[30] R.G. Ewing, D.A. Atkinson, G.A. Eiceman, and G.J. Ewing, "A critical review of ion mobility spectroscopy for the detection of explosives and explosive related compounds," *Talanta*, vol. 54, p. 515, 2001.

[31] F. Röck, N. Barsan, and U.Weimar, "Electronic Nose: Current Status and Future Trends," *Chemical Reviews*, vol. 108, p. 705, 2008.

[32] http://www.smithsdetection.com/IONSCAN_400B.php

[33] A. Smekal, "Zurquantentheorie der dispersion," *Naturwissenschaften*, vol. 11, p. 873, 1923.

[34] C. V. Raman and K.S. Krishnan, “A new type of secondary radiation,” *Nature*, vol. 121, p. 501, 1928.

[35] G. Landsberg and L. Mandelstam, *Naturwissenschaften,* vol. 16, p. 557, 1928.

[36] H.A. Szymanski, “Raman Spectroscopy-Theory and practice,” Buffalo, New York, 1967.

[37] C. Kittel, “Optical Processes and Excitons,” in *Introduction to Solid State Physics*, 8th ed. NJ, John Wiley & Sons, Inc. 1986, ch. 11, p. 344.

[38] T. Vankeirsbilck, A. Vercauteren, W. Baeyens, G. Van der Weken, F. Verpoort, G. Vergote, and J.P. Remon, “Applications of Raman spectroscopy in pharmaceutical analysis,” *Trends in analytical chemistry*, vol. 21, p. 869, 2002.

[39] A. Aponick, E. Marchozzi, C. Johnston, and C.T. Wigal, “Determining the Authenticity of Gemstones using Raman Spectroscopy,” *Journal of Chemical education*, vol. 75, p. 465, 1998.

[40] K. Kneipp, H. Kneipp, I. Itzkan, R.R. Dasari, and M.S. Feld, “Ultrasensitive chemical analysis by Raman Spectroscopy,” *Chemical Reviews*, vol. 99, p. 2957, 1999.

[41] M. Fleischmann, P. J. Hendra, and A. J. McQuillan, “Raman spectra of pyridine adsorbed at a silver electrode,” *Chemical. Physical Letters*, vol. 26, p.163, 1974.

[42] D.L. Jeanmaire and R. P Van Duyne, “Surface Raman spectroelectrochemistry: Part I. Heterocyclic, aromatic, and aliphatic amines adsorbed on the anodized silver electrode,” *Journal of Electroanalytical Chemistry*, vol. 84, p. 1, 1977.

[43] M.G. Albrecht and J.A. Creighton, “Anomalously intense Raman spectra of pyridine at a silver electrode,” *Journal of American Chemical Society*, vol. 99, p. 5215, 1977.

[44] Kneipp K and Kneipp H, “Surface Enhanced Raman Scattering- a tool for ultra sensitive trace analysis,” *Canadian Journal of Analytical Sciences and Spectroscopy*, vol. 48, p. 125, 2003.

[45] M.J. Angebranndt and J.D. Winefordner, “Surface enhanced Raman-spectroscopy on copper hydrosols,” *Talanta*, vol. 39, p. 569, 1992.

[46] J.J. Laserna, “Combining fingerprinting capability with trace analytical detection: surface enhanced Raman spectroscopy,” *Analytica Chimica Acta*, vol. 283, p. 607, 1993.

[47] S. Nie, S.R. Emory, “Probing Single Molecules and Single Nanoparticles by Surface-Enhanced Raman Scattering,” *Science*, vol. 275, p. 1102, 1997.

[48] K. Kneipp, Y. Wang, H. Kneipp, L.T Perelman, I. Itzkan, R.R. Dasari, and M.S. Feld, “Single molecule detection using Surface-Enhanced Raman Scattering,” *Physics Review Letters*, vol. 78, p.1667, 1997.

[49] E.J. Bjerneld, P. Johansson, and M. Käll, “Single molecule vibrational fine-structure of tyrosine adsorbed on Ag nanocrystals,” *Single Molecules*, vol. 3, p. 10, 2000.

[50] H.X. Xu, J. Aizpurua, M. Käll, and P. Apell, “Electromagnetic contributions to single molecule sensitivity in Surface enhanced Raman scattering,” *Physical Review E*, vol. 62, p. 4318, 2000.

[51] H.X. Xu, E.J. Bjerneld, M. Käll, and L. Borjesson, “Spectroscopy of single hemoglobin molecules by surface enhanced Raman scattering,” *Physical Review Letters*, vol. 83, p. 4357, 1999.

[52] M. Moskovits, “Surface Enhanced Spectroscopy,” *Reviews of modern Physics*, vol. 57, p.783, 1985.

[53] K. Kneipp “Surface-enhanced Raman scattering,” *Physics Today*, vol.60, p. 40, 2007.

[54] A. Campion and P. Kambhampati, “Surface enhanced Raman scattering,” *Chemical society reviews*, vol. 27, p. 241, 1998.

[55] P. Mulvaney, “Not all that’s gold does glitter,” *MRS Bulletin*, vol. 26, p. 1009, 2001.

[56] A. Campion, J.E. Ivanecky III, C.M. Child, and M. Foster, “On the mechanism of chemical enhancement in Surface-Enhanced Raman Scattering,” *Journal of American Chemical Society*, vol. 117, p. 11807, 1995.

[57] A. J. McQuillan, “The discovery of Surface-enhanced Raman Scattering,” *Notes and Records of the Royal Society*, vol. 63, p. 105, 2009.

[58] K. Kneipp, “Surface-enhanced Raman scattering,” *Physics Today*, vol. 60, p. 40, 2007.

[59] U. Kreibig and M. Vollmer. *Optical properties of metal clusters*, Berlin, NY: Springer, 1995.

[60] E.C. Le Ru and P.G. Etchegoin, “Principles of Surface-enhanced Raman Spectroscopy and related plasmonic effects,” Wellington, Elsevier, New Zealand, 2009.

[61] M.J. Weaver, S.Z. Zou, and H.Y.H. Chan, “The new interfacial ubiquity of surface-enhanced Raman spectroscopy,” *Analytical Chemistry*, vol.72, p. 38A, 2000.

[62] H. Wackerbarth, C. Salb, L. Gundrum, M. Niederkrüger, K.Christou, V. Beushausen, and W. Viöl, “Detection of explosives based on surface-enhanced Raman spectroscopy,” *Applied Optics*, vol. 49, p.4362 ,2010.

[63] X. Liu, L. Zhao, H. Shen, H. Xu, and L. Lu, “Ordered gold nanoparticle arrays as surface-enhanced Raman spectroscopy substrates for label-free detection of nitroexplosives,” *Talanta*, vol. 83, p. 1023, 2011.

[64] N. Hayazawa, Y. Inouye, Z. Sekkat, and S. Kawata, “Near-field Raman scattering enhanced by a metalized tip,” *Chemical Physics Letters*, vol. 335, p. 369, 2001.

[65] J. Harris, “Autoignition temperatures of Military high explosives by Differential Thermal Analysis,” *Thermochemica Acta*, vol. 14, p. 183, 1976.

[66] S.J. Chang, Y.C. Liu, “Degradation mechanism of 2,4,6-Trinitrotoluene in supercritical water oxidation,” *Journal of Environmental Science*, vol. 19, p. 1430, 2007.

VITA

SUMEDHA TAMANE

Candidate for the Degree of

Master of Science

Thesis: VAPOR-PHASE DETECTION OF EXPLOSIVES BY SURFACE-ENHANCED RAMAN SCATTERING

Major Field: Mechanical and Aerospace Engineering

Biographical:

Personal Data:
Sex: Female
DOB: 08/03/1986
Hometown: Hyderabad, Andhra Pradesh, India

Education:

- Completed the requirements for the Master of Science in Mechanical and Aerospace Engineering at Oklahoma State University, Stillwater, Oklahoma in December, 2011.

- Completed the requirements for the Bachelor of Technology in Mechanical Engineering at Jawaharlal Nehru Technological University, Hyderabad, Andhra Pradesh, India in May, 2008.

Experience:

- Graduate Research Assistant, MAE, OSU, Stillwater (Jan 2010 – July 2011)
- Graduate Teaching Assistant, MAE, OSU, Stillwater (Aug 2008 – Dec 2008)
- Graduate Teaching Assistant, MAE, OSU, Stillwater (Aug 2009 – Dec 2009)

Name: Sumedha Tamane Date of Degree: December, 2011

Institution: Oklahoma State University Location: Stillwater, Oklahoma

Title of Study: VAPOR-PHASE DETECTION OF EXPLOSIVES BY SURFACE-ENHANCED RAMAN SCATTERING

Pages in Study: 62 Candidate for the Degree of Master of Science

Major Field: Mechanical and Aerospace Engineering

In the present work, we employ “nanometal-on-semiconductor” SERS substrates to detect various explosives including TNT, PETN, RDX, and TNB in vapor phase at concentrations on the order of few ppb. The SERS substrates were prepared by a novel process, where a monolayer of surfactant-free Ag nanoparticles was reduced on a Si thin film. Our work also targets a clear understanding of the factors, which so far have limited vapor phase SERS of the explosives. We have identified three major challenges: i) low vapor pressure of explosives at room temperature; ii) weak adsorption of the explosives on Ag nanostructures accounting for easy desorption even under low laser excitation; iii) photochemical decomposition of the explosive under the Raman. The present work also reveals the different adsorption configurations of TNT on Ag nanoparticles using SERS selection rules. The different adsorption configurations are associated with different desorption rates or decomposition rates during the SERS acquisition. We understand that desorption and decomposition of explosives are the major reasons, which have hindered SERS of explosives in vapor phase; previously. Despite the transient nature of the SERS spectrum, we show a reproducible signal is obtainable for 10 s integration. SERS of TNT and other explosives investigated in this study shows reproducible spectral deviations from Raman. This is attributed to chemisorption-induced electron transfer between the TNT molecule and the metal that alters the electron density distribution over the molecule. The nanoparticle temperature measured using Raman scattering as 27 ºC (close to room temperature) suggests that no laser induced heating occurs during our SERS acquisitions and the laser induced decomposition of TNT is a photochemical effect.

ADVISER’S APPROVAL: Dr. A. Kaan Kalkan